Thermal Performance and Corrosion Resistance Analysis of Inorganic Eutectic Phase Change Material with One Dimensional Carbon Nanomaterial

Kalidasan B [a], AK Pandey [a*], R Saidur [a,b], Yogeshwar Nath Mishra [c,d], Zhenjun Ma [e], VV Tyagi [f]

[a)] *Research Centre for Nano-Materials and Energy Technology (RCNMET), School of Engineering and Technology, Sunway University, No. 5, Jalan Universiti, Bandar Sunway, Petaling Jaya, 47500 Selangor Darul Ehsan, Malaysia.*
[b)] *School of Engineering, Lancaster University, Lancaster LA1 4YW, United Kingdom*
[c)] *NASA-Jet Propulsion Laboratory, California Institute of Technology, California 91109, USA*
[d)] *Institute of Engineering Thermodynamics, FAU Erlangen-Nuremberg, DE-91058, Germany*
[e)] *Sustainable Buildings Research Centre, University of Wollongong, Australia*
[f)] *School of Energy Management, Shri Mata Vaishno Devi University, Katra, 182320, (J&K), India*

Abstract

The inherent thermal characteristics, supercooling phenomenon, and corrosion issues associated with salt hydrate phase change materials (PCMs) limit their practical applications. In this research work, we report a newly formulated eutectic salt hydrate PCM using a) sodium sulphate decahydrate (SSD) & b) sodium phosphate dibasic dodecahydrate (SPDD); with a focus on customizing its properties to enhance its suitability for low temperature thermal regulation (achieving a melting point of 27.8 °C and a high heat storage capacity of 215 J/g). Additionally, we have successfully reduced the degree of supercooling and introduced corrosion resistant properties to this PCM. To enhance both the thermal energy transfer rate and optical absorbance of the eutectic PCM, we have incorporated one-dimensional (1D) multiwall carbon nanotube (MWCNT) at various weight fractions, extending up to 0.9%, utilizing a two-step method. The dispersion and chemical stability of SSD/SPDD+MWCNT nanocomposite are verified through the morphological visual and spectral peaks obtained in Fourier transfer infrared spectroscopy. Additionally, studies evaluating the optical and thermal property reveal a substantial 500% increase in absorbance, a notable 77.9% reduction in transmissibility, a thermal conductivity increase from 0.464 W/m·K to 0.742 W/m·K (reflecting a 59.9% increment), and the retention of a consistent melting enthalpy of 218.6 J/g. This stability is attributed to the intermolecular interaction with MWCNT. Similary, the degree of supercooling (ΔT_s) for the SSD/SPDD EPCM containing MWCNT decreased to 2.2 °C from 16.5 °C, marking an 86% reduction compared to the pure eutectic salt solution. Furthermore, this composite demonstrated enhanced thermal and chemical stability throughout 200 thermal

*Corresponding authors: adarshp@sunway.edu.my (AK Pandey)

cycles. Auxiliary ANSYS simulation, with transient boundary condition, are provided to analyze the heat transfer interactions between the thermic fluid and the newly developed PCM when integrated into a thermal regulation system. Subsequently, a corrosion analysis of the developed eutectic PCM and the nanocomposite eutectic PCM exhibits a corrosion rate of 0.018 mpy, well below the permissible level (< 5mpy). The insights gained from the development of this nanocomposite PCM offer valuable guidance for the design and creation of tailored eutectic PCM for low-temperature thermal regulation systems, resulting in significant energy savings.

Keywords: Eutectic Phase Change Material; Multi-wall CNT; Salt hydrate; Thermal Energy Storage; Thermal stability

Highlights

- SSD/SPDD+MWCNT emerges as a promising candidate for low temperature thermal regulation.
- Impact of MWCNTs on the optical & thermodynamic property of the eutectic PCM is assessed.
- Eutectic PCM containing MWCNTs exhibits a reduced degree of supercooling (2.2 °C).
- Corrosion rate for the aluminium sample is 0.018 mpy which is in permissible limit.

53 **Graphical Abstract:**

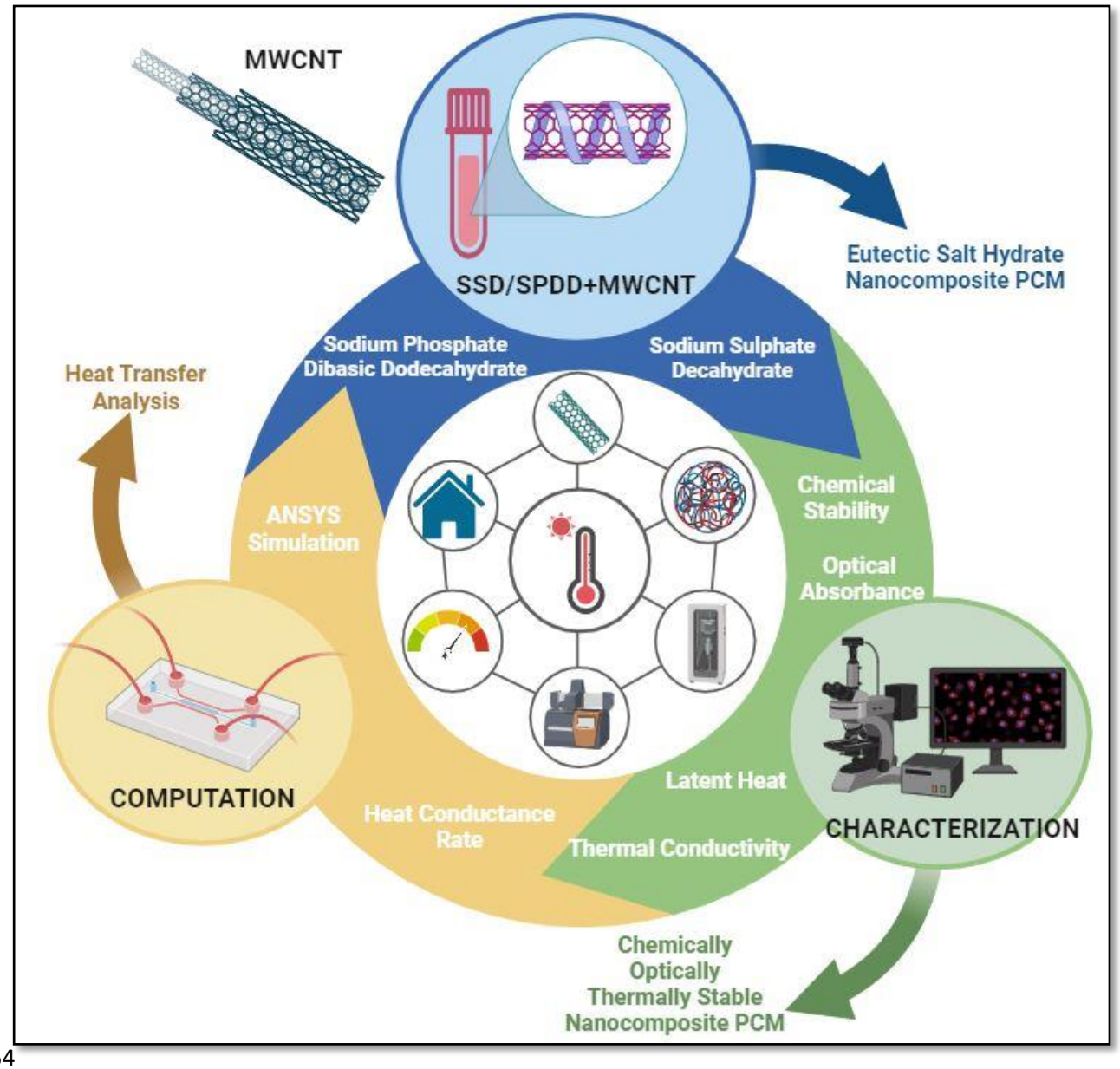

54

1.0 Introduction

The increasing concentration of greenhouse gas emissions and environmental pollution has prompted extensive research into the effective utilization of green and renewable energy sources[1-2]. While the exploration of new renewable energy source has become the primary research focus, equal importance is placed on the development of energy storage devices and systems[3]. Energy storage devices hold promise in bridging the gap between energy demand and supply, facilitating the reliable integration of renewable energy sources for energy consumption[4]. Thermal energy storage (TES) in the form of sensible and latent heat has garnered significant attention over the past decade[5]. One predominant technique employed for storing thermal energy involves the use of phase change materials (PCMs). Fascinated by the ability like a) potential to store energy with wide range of temperature; b) less volumetric expansion; c) high energy density[6] and d) stability over longer service, it is intriguing to explore PCM for TES applications[7]. Nevertheless, PCMs suffer from limitations such as low thermal conductivity, poor optical absorbance, and issues with supercooling[8]. In the meantime, eutectic phase change materials (EPCMs) (combination of two or more PCMs) offer the advantage of developing a) organic-organic EPCM, b) organic-inorganic EPCM, or c) inorganic-inorganic EPCMs tailored to meet the specific thermal requirements of a desired application, thereby overcoming inherent drawbacks. The three unique characteristics of EPCMs are: a) Immiscibility in solid phase, b) Non-reactivity between the components in eutectic mixture and c) Achievability of preferred melting temperature depending on the intended application. The majority of research efforts are focused on the development of binary and ternary EPCMs using organic fatty acids[9] and sugar alcohols[10].

It is well-established that inorganic salt hydrate PCMs possess higher thermal properties and energy density when compared to organic PCMs. Owing to the degree of supercooling (ΔT_s) & phase instability nature, inorganic-inorganic EPCM is of very limited use. On the context, Li et al.[11] in his research work prepared a binary EPCM by mixing $CaCl_2{\cdot}6H_2O$ and $MgCl_2.6H_2O$. They experimented with different weight percentage (ranging from 10-25 wt%) of $MgCl_2.6H_2O$ blended with $CaCl_2{\cdot}6H_2O$ to determine the optimal proportion that exhibited superior thermal characteristics. To address issues related to the degree of phase and supercooling, in the developed EPCM, $SrCO_3$ and $SrCl_2{\cdot}6H_2O$ were blended as nucleating agents, and hydroxyethyl cellulose was included as thickener. The supercooling of $CaCl_2{\cdot}6H_2O$ was observed at a temperature of 17 °C, while the phase transition temperature was 23.7°C. The results showed that a mixture of $CaCl_2{\cdot}6H_2O$:$MgCl_2.6H_2O$ at a ratio of 75:25 wt% resulted in eutectic melting of 21.7 °C with a latent heat of 102 J/g.

However, the eutectic PCM only exhibited a reduction in the degree of supercooling by 2 °C. In another work, Zhang et al.[12] dispersed expanded perlite with the eutectic mixture of magnesium chloride hexahydrate and calcium chloride hexahydrate to investigate its chemical and thermal stability. The results ensure a drop in latent heat to 73.55 J/g, accompanied by a significant reduction in thermal conductivity from 0.732 W/m·K to 0.144 W/m·K. Meanwhile, the developed eutectic exhibited good thermal reliability over an extended service life. A deep eutectic solvent consisting of choline chloride and calcium chloride hexahydrate was developed by Shahbaz et al.[13] for the purpose of thermal regulation in buildings. The deep eutectic solvent offered an energy storage potential of 130 J/g with a melting point of 23 °C. Liu and Yang[14] prepared an EPCM mixture using $Na_2SO_4 \cdot 10H_2O$ and $Na_2HPO_4 \cdot 12H_2O$, operating at 31.2 °C, with a focus on solar heating units. To further enhance the thermo physical properties, Al_2O_3 was dispersed. The results depict a reduction in supercooling from 7.8 °C to 1.6 °C, along with a significant decrease in melting enthalpy. Similarly, Fang et al.[15] prepared a binary EPCM of $Na_2SO_4 \cdot 10H_2O$ and $Na_2HPO_4 \cdot 12H_2O$ by substituting weight fractions of $Na_2HPO_4 \cdot 12H_2O$ with 15% and 20% of $Na_2SO_4 \cdot 10H_2O$ to establish the ideal eutectic mixture ratio. By incorporating 2.5 wt% of $Na_2SiO_3 \cdot 9H_2O$ as a nucleating agent and 30 wt% porous fumed silica, they achieved a 31.9% reduction in energy storage capacity while successfully creating a foam-stable PCM. A binary eutectic PCM of $Na_2SO_4 \cdot 10H_2O$ and $Na_2HPO_4 \cdot 12H_2O$ was mixed at 1:4 mass ratio with SiO_2 nanoparticles and Na_2SiO_3 was used as silica precursor[16]. The objective was to create a shape-stabilizing PCM, and a novel preparation method was employed. It was observed that this preparation technique led to a significant reduction in latent heat to 27.3 J/g. Liu et al.[17] attempted to prepare an economically viable shape-stabilized PCM using fly ash as a carrier material, incorporating a binary EPCM of $Na_2SO_4 \cdot 10H_2O$+$Na_2HPO_4 \cdot 12H_2O$ mixed at a ratio of 69:25 wt%. The proportion of $Na_2SO_4 \cdot 10H_2O$ with $Na_2HPO_4 \cdot 12H_2O$ was determined through a trial and error method, by substituting $Na_2HPO_4 \cdot 12H_2O$ with 10%, 15%, 20%, 25%, 30%, 35%, and 40% of $Na_2SO_4 \cdot 10H_2O$. Additionally, 2wt% & 4wt% of carboxymethyl cellulose (CMC) were respectively used to address phase instability and reduce the ΔT_s. The prepared fly ash based EPCM showed an energy storage capacity 106.9 J/g. Utilising $Na_2SO_4 \cdot 10H_2O$ and $Na_2HPO_4 \cdot 12H_2O$, Xin et al.[18] also created an inorganic eutectic PCM. The primary objective was to ascertain how nucleating and thickening agents influenced the ΔT_s and phase instability. The combination of borax and aluminium nitride powder (AIN) with a 1.8% nm size resulted in a reduction of supercooling to 3.1 °C. Liu et al.[19] prepared a binary eutectic PCM with a 40:60 wt% ratio of $Na_2CO_3 \cdot 10H_2O$ to $Na_2HPO_4 \cdot 12H_2O$. The main objective of this study was to analyze the thermophysical characteristics of the binary eutectic

PCMs. In this study, the ratio of $Na_2CO_3 \cdot 10H_2O$ to $Na_2HPO_4 \cdot 12H_2O$ was determined using a trial-and-error method by substituting various amounts of $Na_2CO_3 \cdot 10H_2O$ for $Na_2HPO_4 \cdot 12H_2O$: 10%, 20%, 30%, 40%, 50%, 60%, and 70%, respectively. It should be noted that the Schrader equation, typically used for eutectic mixtures, did not apply to this specific eutectic percentage. The goal of the study was to formulate a binary eutectic PCM using $Na_2CO_3 \cdot 10H_2O$ and $Na_2HPO_4 \cdot 12H_2O$ and evaluate the reduction in supercooling at heating rates of 5 °C/min and 1 °C/min, resulting in temperature of 15.8°C & 3.6°C. Furthermore, Liu and Yang[20] investigated on the thermal performance enhancement of the $Na_2CO_3 \cdot 10H_2O$ and $Na_2HPO_4 \cdot 12H_2O$ EPCM by incorporating expanded graphite oxide. They observed a lower degree of supercooling attributed to the abundance of surface oxygen functional groups and surface defects. The developed nanocomposite sample exhibited thermal stability through 200 thermal cycles. Wu et al.[21] developed a binary EPCM of $Na_2SO_4 \cdot 10H_2O$+$Na_2HPO_4 \cdot 12H_2O$ at a 50:50 wt% mixture, although they did not provide an explanation for the mass ratio proportion between $Na_2SO_4 \cdot 10H_2O$ and $Na_2HPO_4 \cdot 12H_2O$. To improve the thermal properties and stability of EPCM, they used 14.2 wt% of expanded graphite (EG), 4 wt% of borax & 2 wt% of CMC as a nanoparticle, nucleating agent and thickening agent respectively. To solve the challenges of phase instability and leakage, Xie et al.[22] developed a form-stable PCM with a polyurethane coating. In this study, they selected a eutectic mixture of sodium carbonate decahydrate and disodium hydrogen phosphate dodecahydrate as a PCM. Upon evaluation, the melting enthalpy of the stable PCM was determined to be 102.6 J/g, and it exhibited a negligible degree of supercooling. Furthermore, when subjected to a thermal cycling test and analysed using a thermogravimetric analyzer (TGA), the results demonstrated excellent thermal reliability and stability. Similary, Zhang et al.[23] developed a shape-stabilized PCM by utilizing waste plastics as a supporting material to address phase instability and prevent leakage issues. Nonetheless, the application of plastic as a supporting material in combination with inorganic PCM has not been extensively explored yet. In another study, Ling et al.[24] prepared an EPCM using $MgCl_2.6H_2O$ and $Mg(NO_3)_2.6H_2O$ for solar water heating application. This EPCM has a eutectic temperature of 58 °C and enthalpy of 127 J/g. To further enhance the thermal property of the developed EPCM, SiO_2 nanoparticles were dispersed, and results showed only a 5% increment in thermal conductivity. Xie et al.[25] conducted an investigation by impregnating a eutectic mixture of $Na_2SO_4 \cdot 10H_2O$ and $Na_2CO_3 \cdot 10H_2O$ into expanded vermiculite. The resulting nanocomposite exhibited a phase transition temperature of 24 °C with a heating enthalpy of 110.3 J/g. Zou et al.[26] developed a shape-stabilized PCM with a superabsorbent polymer as the outer coating and a eutectic mixture of $Na_2HPO_4 \cdot 12H_2O$ & $K_2HPO_4 \cdot 3H_2O$.

They conducted an evaluation of various thermophysical characteristics of the nanocomposites , including melting temperature, thermal stability, supercooling, and thermal conductivity. The results showed a negligible degree of supercooling, a melting temperature of 24.13 °C, a melting enthalpy of 172 J/g, and a thermal conductivity of 0.474 W/m·K. However, it is worth noting that EPCMs operating at lower temperature with a melting enthalpy of 200 J/g or higher are rarely reported to date, and the impact of carbon nanoparticles on enhancing thermophysical characteristic in such EPCMs remains largely unexplored.

Based on the literature discussed, it is evident that significant research experiments have been conducted in the development of EPCMs using organic fatty acids[9], sugar alcohol-based eutectic mixtures[10], and salt hydrate EPCMs with inorganic salt hydrate PCMs. However, there is a notable gap in the exploration of the energy storage potential of inorganic salt hydrate-based EPCMs operating at low temperatures with high melting enthalpy. This gap exists primarily due to three challenging issues that hinder the practical application of salt hydrate PCMs: (1) non-tunable thermal characteristics (or thermophysical properties), including a fixed latent heat and low thermal conductivity, (2) their corrosive nature, and (3) the problem of supercooling. Upon careful examination, it is inferred that EPCM, owing to its structural differences, marginal density variations, and crystallisation behaviour, is expected to substantially reduce the degree of supercooling. Since the eutectic mixture percentage was determined through a trial-and-error approach, it's important to note that the inorganic-inorganic binary eutectic PCM composed of $Na_2SO_4 \cdot 10H_2O$ and $Na_2HPO_4 \cdot 12H_2O$ developed by the researchers does not conform to the Schrader equation. In contrast, varying ratios of the eutectic mixture are employed for like combinations of salt hydrate PCM to achieve a single phase transition temperature. To tackle the previously mentioned issue, the authors employ the Schrader equation to calculate the eutectic composition. Subsequently, they experimentally prepare the PCM using the calculated eutectic ratio to decide the thermophysical characteristics. The eutectic ratio of sodium phosphate dibasic dodecahydrate and sodium sulphate decahydrate differs from the results of previous investigations. In this study, we created a novel eutectic nanocomposite PCM consisting of two salt hydrates: a) sodium sulphate decahydrate (SSD) & b) sodium phosphate dibasic dodecahydrate (SPDD), along with multi-walled carbon nanotube (MWCNT) nanoparticles. This PCM is designed to operate at a temperature of 27.8 °C and possess a melting enthalpy of 215 J/g, as calculated using the Schrader equation. MWCNTs offer significant advantages due to their large aspect ratio and surface area. They also facilitate the formation of well-developed thermal networks, thanks to their inherently high thermal conductivity. The aim of the current experimental research is to

expedite the enhancement of thermal conductivity in the binary EPCM, improve optical absorbance, and address the issue of supercooling by incorporating MWCNTs. The developed nanocomposite PCM has undergone experimental characterization, including the assessments of its morphological and chemical stability, optical absorbance and transmissibility, energy storage potential, phase transition temperature, thermal conductivity, degree of supercooling, and thermal stability. Inspired by the promising thermal and optical properties, as well as the stability of the developed nanocomposite PCM, we conducted heat transfer performance analysis using ANSYS simulation. This analysis aims to provide a deeper insights into the solidification and melting processes of the developed binary eutectic PCM within thermal energy storage units. Additionally, we conducted a corrosion analysis to assess the corrosion rate of aluminium plate exposed to the salt hydrate eutectic PCM over a 90-day period. Our research endeavours in formulating and developing this unexplored combination of EPCM are expected to pave the way for innovative research in sustainability and enhance the opportunities for the commercialization of PCM technology.

2.0 Experimental Section

2.1 Materials

Salt hydrate sodium sulphate decahydrate ($Na_2SO_4.10H_2O$) (99% purity) having a molar mass of 322.19 g/mol and sodium phosphate dibasic dodecahydrate ($Na_2HPO_4.12H_2O$) (99% purity) having a molar mass 358.1 g/mol, used for the research exploration were procured from Sigma Aldrich (Germany). MWCNT with inner and outer diameter of 5-10 nm and 10-20 nm, used in this investigation was purchased US Research Nanomaterials, Inc. Other physical characteristic of MWCNT includes, length to be 10-30 μm, specific surface area of 200 m^2/g with 2100 kg/m^3 density. The manufacturing technique involved in preparation of MWCNT nanoparticle was chemical vapour deposition.

2.2 Design procedure for development of SSD/SPDD eutectic mixture ratio

The point at which two or more components undergo phase transition identically is termed as eutectic melting point, and the corresponding proportion of the component is the eutectic mixture weight fraction. In general, binary EPCM, involves two base component, ternary EPCM involves three base PCM component and so on. This section provides information on the procedure to determine the eutectic point and eutectic mixture ratio of the salt hydrate PCM component opted in this research. In this research investigation the major focus is on developing a binary EPCM (involving two components) for low temperature application. Phase transition of any PCM is expected to be isothermal in nature with a fixed

phase transition point, as it is very predominant factor to be consider while developing an EPCM. In general, the, eutectic point of any two components can be designed by a) prediction testing method (Phase diagram) and b) proportion testing method [Differential Scanning Calorimetry (DSC) instrument]. Considering the number of samples to be tested in DSC, and to minimize the cost we adopt the numerical prediction method with the help of Schroeder-Van Laar equation[27] to determine the eutectic point. The binary eutectic melting point and its associated proportion, the eutectic mixture ratio, are the points where the curves of the two concerned components overlap. A variant of the phase equilibrium concept[28] is the Schrader equation as in (1) and (2) that offers a correlation between the thermal properties of the planned eutectic mixture at altered compositions.

$$T_m = \left[\frac{1}{T_{0,A}} - R.\frac{lnX_A}{\Delta H_{m,A}}\right]^{-1} \quad (1)$$

$$T_m = \left[\frac{1}{T_{0,B}} - R.\frac{lnX_B}{\Delta H_{m,B}}\right]^{-1} \quad (2)$$

Note: T_m denotes the binary eutectic mixture's melting point in Kelvin; $T_{0,A}$ and $T_{0,B}$ denotes the onset melting points of components A and B in Kelvin; and X_A and X_B denotes the eutectic mixture's proportion in mole percent. The melting enthalpy of components A and B is shown by the symbols $\Delta H_{m,A}$ & $\Delta H_{m,B}$ in kJ·kmol^{-1}. In the aforementioned equations (1) and (2), the gas constant, R, is indicated and equals 8.314 kJ·kmol^{-1}·K^{-1}. The melting enthalpy during phase transition is a crucial thermophysical characteristic of the planned EPCM and is calculated using equation (3)[29]

$$H_{eu} = T_{eu}.\sum_{i=1}^{n}\left[\frac{X_i.H_i}{T_i} + \left\{X_i.(Cp_{li} - Cp_{si}).ln\frac{T_{eu}}{T_i}\right\}\right] \quad (3)$$

Note: H_{eu} and T_{eu} stand for the eutectic mixture's melting enthalpy and melting temperature in kJ·mol^{-1} and K, respectively; X_i stands for the component i's fraction in mole percent. Additionally, C_{pli} & C_{psi} which are expressed in kJ·kg^{-1}C^{-1}, are the specific heat capacity in both the solid and liquid states.

2.3 Preparation of MWCNT dispersed binary EPCM

Solid inorganic salt hydrate PCM crystal of SSD and SPDD at a weight ratio of 62% and 38% as designed and calculated using Schrader equation is weighed and taken to develop binary EPCM experimentally. SSD and SPDD were precisely weighed as per the aforementioned proportion and heated using a hot plate at 60 °C as illustrated in Figure 1. To ensure homogenous mixture, the melted eutectic mixture is sonicated using bath sonicator for 30 minutes. Now to further boost the thermal conductive nature, optical absorptivity and

thermal reliability of the developed EPCM, MWCNT nanoparticles are interpenetrated within the eutectic mixture. In the current investigation, MWCNT nanoparticles are dispersed and penetrated with SSD/SPDD eutectic mixture at weight fraction of 0.1%, 0.3%, 0.5%, 0.7% and 0.9%. Initially 20 g of the above-developed SSD/SPDD EPCM is weighed and mixed with 0.02 g of MWCNT nanoparticle in the liquid state PCM. The composite mixture consisting of MWCNT and SSD/SPDD were sonicated with the help of water bath sonicator for 60 minutes with caution to ensure that the nanotubes are not damaged. To ensure no chemical reactions to be taken place between the composite, the samples are further investigated using IR spectroscopy. SSD/SPDD EPCM samples with MWCNT of 0.1%, 0.3%, 0.5%, 0.7% and 0.9% is symbolized as SSD/SPDD+0.1MWCNT, SSD/SPDD+0.3MWCNT, SSD/SPDD+0.5MWCNT, SSD/SPDD+0.7MWCNT & SSD/SPDD+0.9MWCNT, respectively. In addition to the preparation technique (Supplementary S1; Appendix I) also provides the granular structure visuals of a) SSD, b) SPDD & c) SSD/SPDD EPCM for better understanding of the inorganic salt hydrate PCM morphology. Details in regard to sensitive instruments and characterisation techniques are provided in (Supplementary; Appendix II).

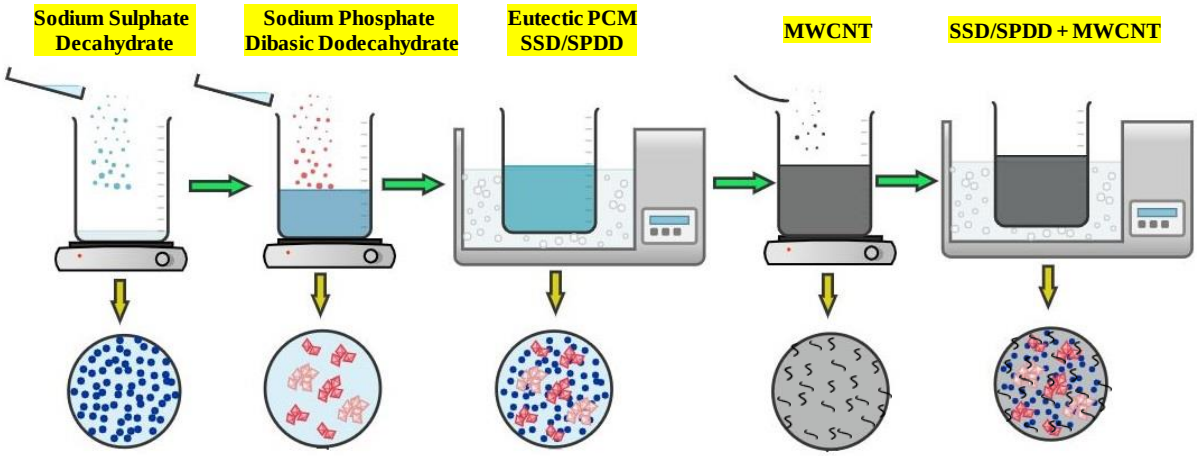

Figure 1: Detailed preparation procedure of SSD/SPDD binary EPCM with dispersion of MWCNT

2.4 Boundary Condition for Numerical Simulation of Solidification/Melting of composite PCM

ANSYS simulated numerical analysis of the developed MWCNT@SSD/SPDD EPCM composite is conducted to evaluate the solidification and melting process of the developed nanocomposite on real time thermal energy transfer system. In this analysis thermic fluid (H_2O) is heated with the help of developed MWCNT@SSD/SPDD, the inlet fluid temperature is considered to be 293 K (20 °C) with mass velocity of 0.05 kg/s. Thermic fluid and PCM are in concentric tube as in Figure 2, using which a 3D transient simulation is conducted. The

dimensions of the concentric tubes are, thermic fluid carrying pipe with inner diameter 25 mm with 1 mm thickness, and PCM filled pipe with inner diameter of 50 mm and 1 mm thickness. The outer surface of the PCM filled tube at a temperature of 320 K (47 °C) is maintained constant. The material properties of the binary EPCM and nanocomposite EPCM is provided in (Supplementary T1-T2; Appendix III).

3.0 Results and Discussion

In this research investigation morphological, chemical, optical and thermal behaviours of the state-of-the-art low temperature salt hydrate PCM is analysed by penetrating one-dimensional MWCNT nanoparticles. Insightful observations, inferences and results are discussed below:

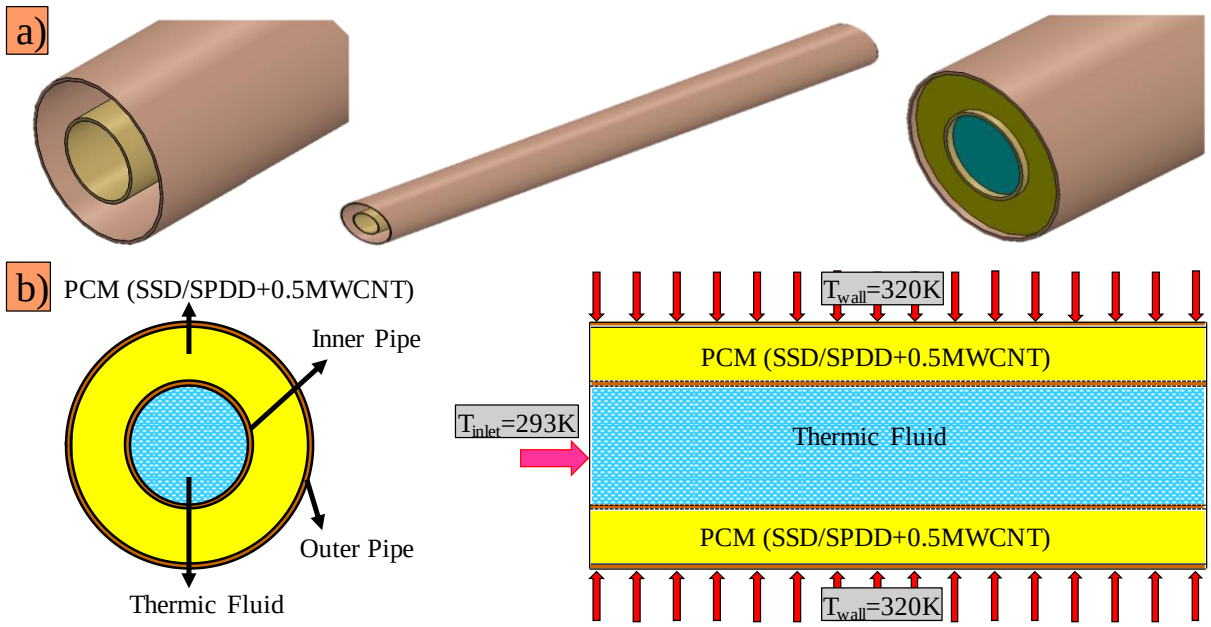

Figure 2: a) Model of concentric pipe with thermic fluid and charged nanocomposite PCM; b) Boundary condition and lateral view of the concentric tube

3.1 Theoretical aspects of formulation of binary EPCM

In accordance with the design process described in Section 2.2, we formulate and developed a binary eutectic composition for estimating the eutectic melting point (T_{eu}) and melting enthalpy (ΔH_{eu}). The phase diagram of a binary eutectic mixture is shown in Figure 3a, where the abscissa indicates the salt hydrate's composition (SSPD on the left and SSD on the right) and the ordinate the salt hydrate's phase transition temperature. The onset melting temperatures of SPDD and SSD are 37 °C and 33 °C, respectively, as inferred from Figure 3a. Eutectic point is determined by varying the proportion of SSD with SPDD, increasing SSD composition with SPDD, reduces the phase transition temperature of SPDD and it occurs vice

versa with SPDD mixture with SSD. Until a common intersection is found, this composition is changed. The eutectic point is the location, where the eutectic SSD/SPDD mixture melts simultaneously. The eutectic mixture ratio, or composition that corresponds to the eutectic point, is identical to 62% SSD & 38% SPDD. The solid-liquid phase of the eutectic mixture is indicated by the line, which represents the phase transition curve. It is clear that the T_{eu} (27.8 °C) for eutectic mixtures are lesser than the onset T_m of pure salt hydrates (T_m=33 °C for SSD & T_m=37 °C for SPDD), which is attributed because of the increase in impurity, where an increase in entropy generation tends to lower the melting point of mixture[30-31]. According to the Gibbs free energy (ΔG°) equations , the variations in enthalpy and variation entropy have an unfavourable impact on the value of ΔG°. While change in entropy is the contributing factor that results in a lower eutectic point than pure salt hydrate, change in enthalpy is practically identical for a pure and impure solid due to the equal intermolecular force[32]. Atomic mobility among solid-state molecules results in very less variation in entropy, whereas increased disorder in liquids results in higher variation in entropy. The eutectic PCMs' decreased melting enthalpy is explained by this phenomenon. Phase transition from salt to liquid happens when the eutectic binary combination is heated above the eutectic point. Therefore, the ability of PCMs to store heat energy, or latent heat, is another important thermal feature to take into consideration when choosing or creating a eutectic mixture PCM. The aforementioned equation (3) is used to calculate the latent heat of the EPCMs, as shown in Figure 3b, along with the eutectic compositions of each material on the X-axis. According to a numerical evaluation, the binary EPCM SSD/SPDD is designed to have a latent heat value of 215 J/g. Compared to SSD and SPDD, the enthalpy of SSD/SPDD (215 J/g) is slightly less at the eutectic percentage. It is important to note that the impure solid (a mixture of two or more components) results in an increase in free energy (G°), entropy generation, and a minor decrease in the latent heat of the formed EPCM.

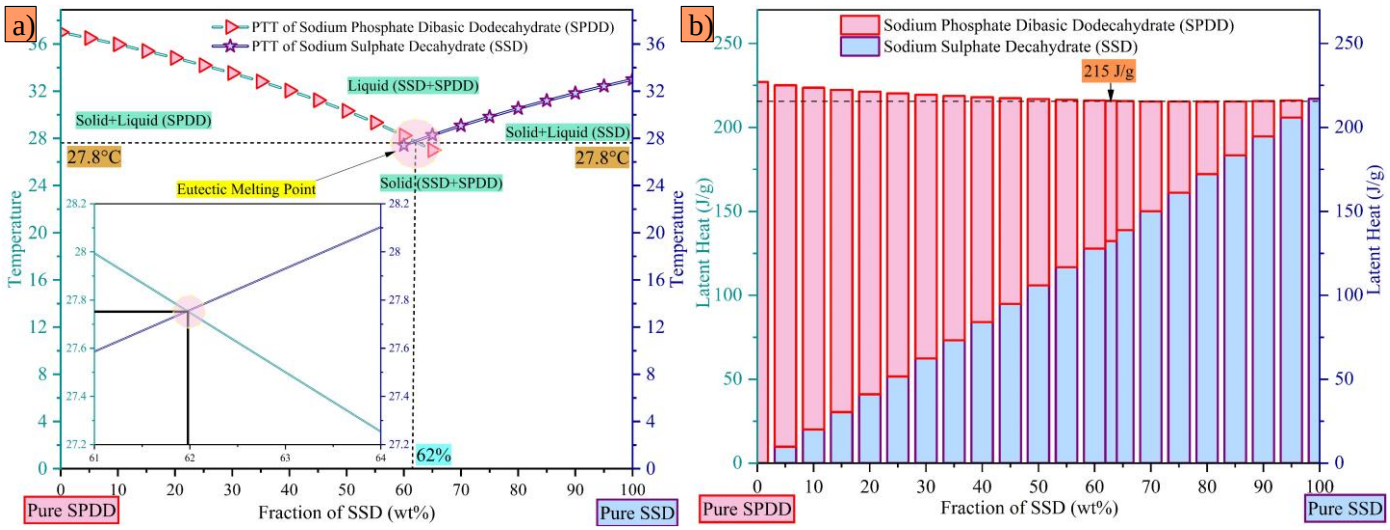

Figure 3: a) Eutectic melting point of SSD/SPDD b) Heat storage enthalpy bars of SSD/SPDD at different eutectic ratio.

3.2 Morphological analysis of MWCNTs, SSD, SPDD and SSD/SPDD/MWCNT composites

The scanning electron microscope (SEM) images of nanoparticle (MWCNT), low temperature pure salt hydrates SSD and SPDD, developed binary EPCM (SSD/SPDD) and the nanoparticle dispersed EPCMs (SSD/SPDD+MWCNT) are exposed in Figure 4. SEM profile of the procured MWCNT were depicted to analyse the microscopic structure of the nanoparticle. It can be inferred from the visuals in Figure 4a that the MWCNT nanoparticles are, one dimensional thread like structure of tangled bundled with uniform size and shape. MWCNT is beneficial as they exhibit large aspect ratio and surface area, as well supports formation of well-developed thermal networks owing to their higher thermal conductivity nature. In addition, the authors have provided the morphological visuals of SSD and SPDD captured using cold storage facility due to the low melting point of the salt hydrates. In Figure 4b the SEM visual of SSD shows very tiny pores and micro structured spherical balls clustered together, as well SPDD in Figure 4c exhibits a granular crystal with cubical bar structure. Also Figure 4d shows the SEM image of 62% of SSD and 38% SPDD in solid state. The salt hydrate EPCM consists of tiny pore of spherical ball clusters signifying the existence of SSD and granular structure cubical bar like structure ensuring the presence of SPDD. It can also be observed that the presence of SPDD in eutectic mixture is more like corrugated sheets[19] of cubical shape as can be closely viewed as Figure 4e. The changes between the pure base and the eutectic mixture might be owing to the reason that with interaction between the hydrated salts during new crystal growth their might be changes in surface energy resulting in size and shape of the crystal[33]. Additionally, Figure 4e also delivers the existence of MWCNT dispersed

salt hydrate EPCM. In most existing literature, the presence of nanoparticle specifically MWCNT irrespective of the melting point of the base PCM is not well visualized. However, the present SEM results will attract researchers to explore further and understand the thermal network propagation of MWCNT, and crystal growth of low temperature salt hydrate EPCMs.

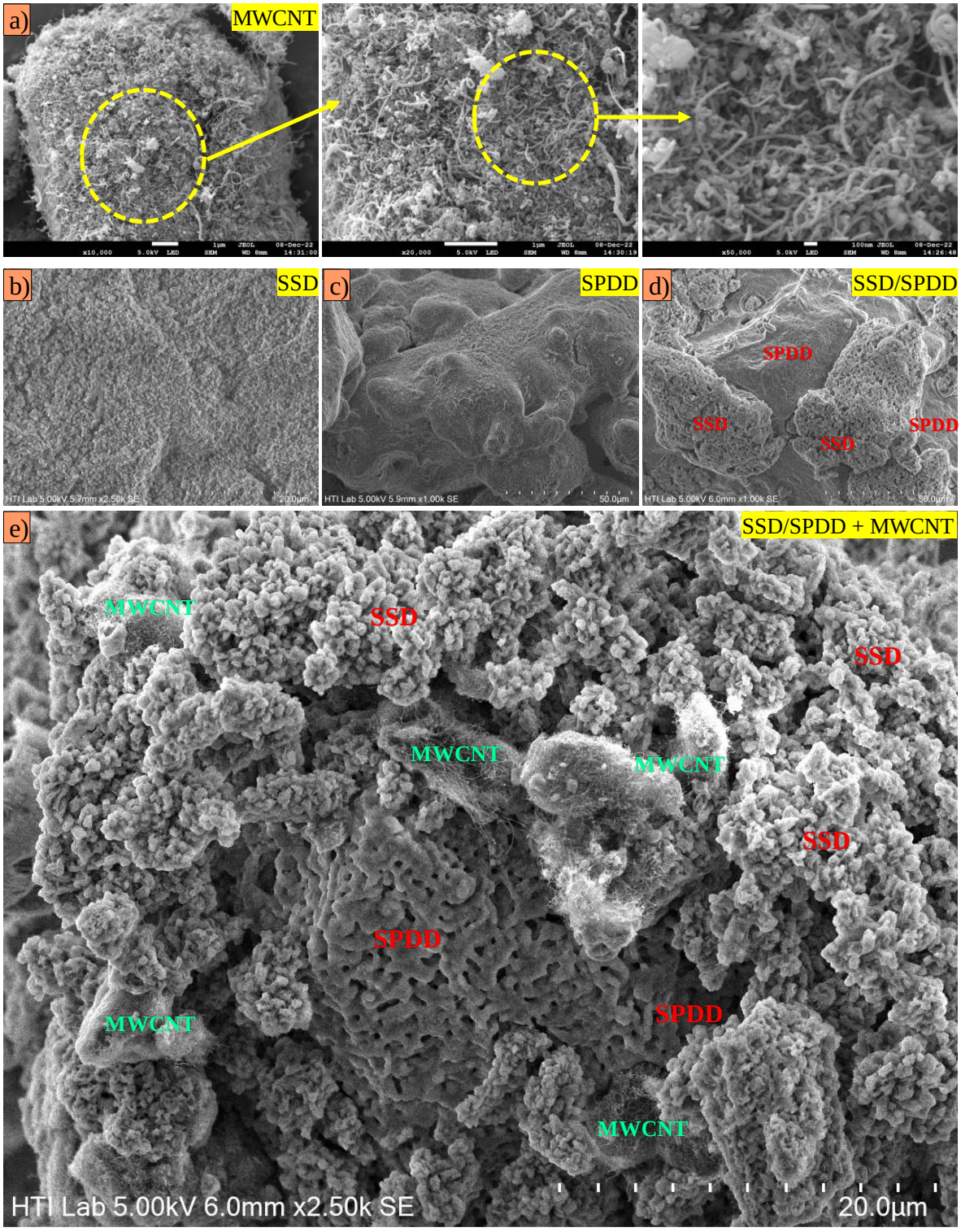

Figure 4: Morphological visuals of a) MWCNT, b) SSD, c) SPDD, d) SSD/SPDD eutectic composite and e) MWCNT distributed SSD/SPDD binary EPCM composite

3.3 Spectral Peak analysis

Chemical stability of binary EPCM (SSD/SPDD) and its MWCNT dispersed nanocomposite of are investigated using FTIR spectral peaks. Figure 5 shows the FTIR spectral peaks of salt hydrates a) SSD, b) SPDD; the developed binary EPCM (SSD/SPDD); and various nanocomposite of the developed EPCM with MWCNT at various weight percent. To begin with, the FTIR spectral curve for SSD salt hydrate PCM is analysed. Three sharp peaks in the finger group region at wavenumber 1082 cm^{-1}, 618 cm^{-1} & 487 cm^{-1}; and two wide band at function group region is noticed, the former strong peak at wavenumber 3250-3550 cm^{-1} and later a weak peak at wavenumber 1605-1710 cm^{-1}. Sharp absorption peak of SO_4^{2-} with asymmetric stretching vibration is noticed around 1082 cm^{-1}. Another asymmetric angular absorption peak of SO_4^{2-} is noticed around 618 cm^{-1} and 487 cm^{-1} [34]. Former wider peak around 3250-3550 cm^{-1} indicates the stretching vibration of the water molecule[35]. Meanwhile, the later weak peak around 1605-1710 cm^{-1} represents the rocking and scissoring angular vibration of water molecule. Likewise, spectral curve of SPDD salt hydrate PCM depicts three peaks (sharp peak at 1074 cm^{-1} & 987 cm^{-1} in the finger group region and a wide peak around 2900-3600 cm^{-1} at the functional group region). Wide peak 2900-3600 cm^{-1} indicates the O-H vibration peak due to water molecule crystallisation[36]. And the sharp peak at 1074 cm^{-1} denotes the P-O stretching vibration and peak at 987 cm^{-1} denotes the PO-H bending vibrational peak[37].

FTIR spectral curve of the developed binary EPCM indicates sharp peaks in finger group region around wavenumber 487 cm^{-1}, 618 cm^{-1}, 987 cm^{-1} and 1078 cm^{-1}. Equally it also produces a weak wide peak around 1605-1714 cm^{-1} and an intense wide peak around wavenumber 2960-3580 cm^{-1}. It can be inferred that all spectral peaks observed in pure salt hydrate PCM sample SSD and SPDD are seen in the developed binary EPCM (SSD/SPDD) ensuring the proper formation of the newly developed PCM. Additionally, all the nano composite SSD/SPDD+MWCNT with various weight fraction ensures the availability of similar peaks present in the developed EPCM. Moreover, no new sharp or wide peaks are observed in the nano composite of MWCNT penetrated EPCM, which also ensures no chemical reaction to occur and the samples are physically mixed.

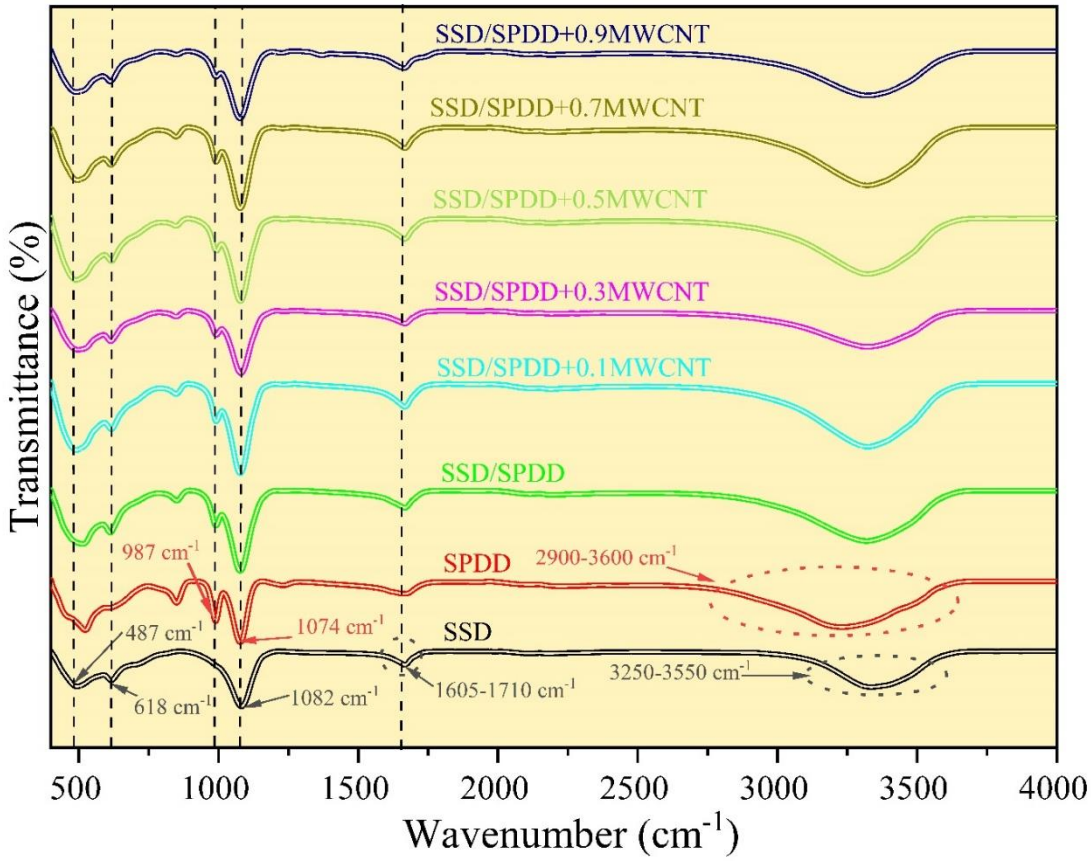

Figure 5: FT-IR spectra of pure SSD, SPDD salt hydrate and SSD/SPDD+MWCNT composites

3.4 Optical property of MWCNT dispersed binary EPCM

In this section, the photo optical absorptivity and transmissibility of MWCNT nanoparticle penetrated SSD/SPDD binary EPCM is analysed. Monochromatic beam of light rays is passed to the solid sample specimen using UV-Vis spectroscopy to assess the absorbance and transmittance characteristics. Figure 6 presents the absorbance and transmissibility nature of SSD/SPDD+MWCNT nanocomposite samples at various weight percentage in the wavelength of 280 nm to 1400 nm. Commonly solar energy consists of three maximum available regions namely a) Ultraviolet (280–380 nm) b) Visible region (380–740 nm) and c) Near infrared (740–1400 nm). From Figure 6a it is clear that pure salt hydrate PCMs, SSD (0.16 absorbance) and SPDD (0.22 absorbance) exhibit lower absorbance Likewise, due to excess water content and lowered melting point the developed SSD/SPDD EPCM display a lower of 0.13 absorbance within the wavelength 280-1400 nm. Nevertheless, with penetration of MWCNT within the surface of SSD/SPDD better increment in absorbance of solar radiation is observed in Figure 6a. MWCNT at weight percentage of 0.1 wt%, 0.3 wt%, 0.5 wt%, 0.7 wt% and 0.9 wt% with SDD/SPDD enhances the absorbance to 0.48, 0.531, 0.56, 0.64 and 0.78, respectively. This is ascribed by the active nature of MWCNT in the UV-Vis

region owing to ID Van Hove singularities[38]. In case of bundled MWCNT, the photoluminescence gets quenched due to the bundling and tunnelling between the nanotubes and replicates in lower absorbance of radiation[39]. Hence, absorbance of solar radiation with in the UV region is directly proportionate to the extent of de-bundled MWCNT. In addition, penetration of MWCNT within the developed SSD/SPDD EPCM, reveal a darker coloured nature of the nanocomposite compared to the EPCM and contributes for better absorbance[40].

Most PCMs are transmissible in nature owing to the white surface texture. It can be understood from the transmissibility curves in Figure 6b that, increase in proportion of MWCNT penetration with SSD/SPDD effectively contribute in reducing the transmittance of light radiation. As absorbance and transmittance are inversely proportional, increase in absorbance has resulted in decrease in transmittance nature. On further calculation and validation with the data from Gueymard[41], the transmittance percentage of developed SSD/SPDD EPCM is 74.2%. Similarly, for MWCNT dispersed SSD/SPDD at weight percentage of 0.1 wt%, 0.3 wt%, 0.5 wt%, 0.7 wt% and 0.9 wt% with SSD/SPDD salt hydrate is 33.5%, 28.8%, 27.55%, 22.1% and 16.4% correspondingly.

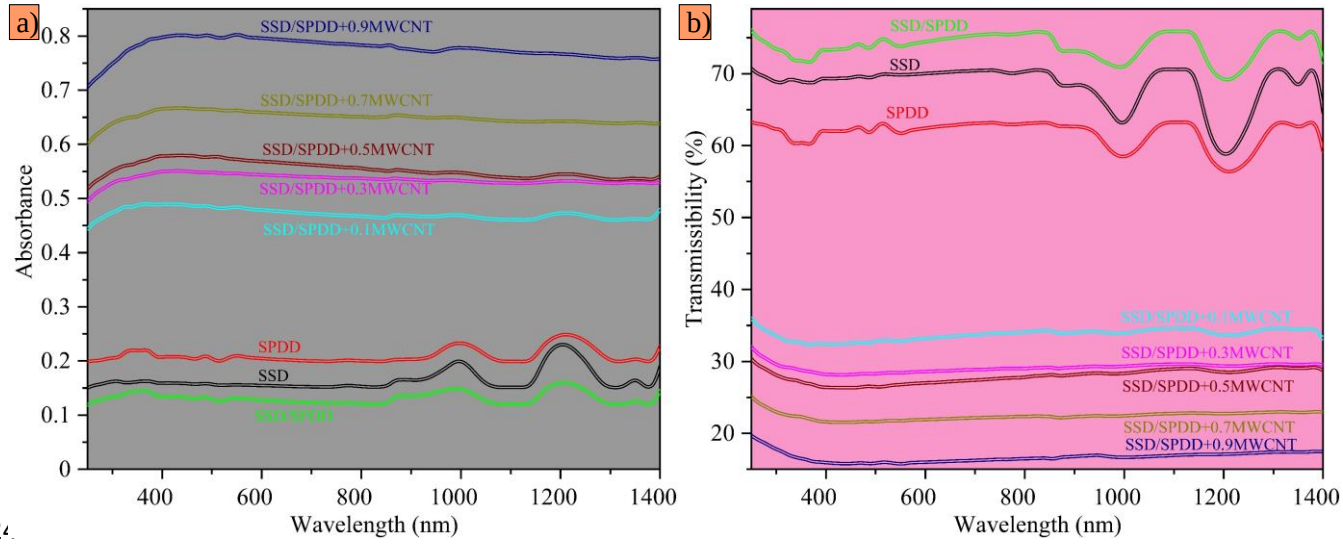

Figure 6: UV Vis spectroscopy analysis of SSD/SPDD+MWCNT samples a) Absorbance & b) Transmittance

3.5 Thermal conductivity of SSD/SPDD/MWCNT and enhancement mechanism

TES of the prepared salt hydrate EPCM, significantly depends on its thermal conductive nature. Rate of energy storage in PCM is desirable based on the thermal conductive of the PCM. Though inorganic PCM, exhibit higher thermal conductivity compared to organic PCM, any further improvement is expected to make remarkable contribution with energy storage application. Figure 7 presents the heat transfer enhancement mechanism on penetration MWCNT with SSD/SPDD; in addition, it also depicts the thermal conductivity of SSD/SPDD+MWCNT at various weight percent. The interaction between nanomaterials and the base PCM matrix are of utmost importance to understand the heat transfer enhancement mechanism. On a whole, the intermolecular thermal resistance is high in case of base PCM, and dispersion of nanomaterial will form well-developed thermal network overcoming the thermal resistance. It can be discussed schematic using Figure 7a, the role of MWCNT nanomaterial is establishing thermal network. On a whole the dispersed MWCNT is a reliable filler to improve the conductive nature and in establishing a support for effective crystallization owing to its higher thermal conductivity of 2000-600 W/m·K[42]. The one dimensional, thread shaped MWCNT on dispersion with SSD/SPDD EPCM, effectively penetrates the surface of SSD/SPDD and creates a better interconnected networks for heat transfer to occur. Nevertheless at higher proportion the MWCNT bundles themselves, forms cluster and quenches and fails to develop thermal network, henceforth the proportion of MWCNT in the prepared SSD/SPDD salt hydrate EPCM is noteworthy. Figure 7b displays the increase in thermal conductivity of nano composite SSD/SPDD+0.1MWCNT, SSD/SPDD+0.3MWCNT, SSD/SPDD+0.5MWCNT, SSD/SPDD+0.7MWCNT and SSD/SPDD+0.9MWCNT. The developed binary EPCM exhibit a thermal conductivity of 0.464 W/m·K. On dispersion of MWCNT, the thermal conductivity of the nano composite increases until 0.5 wt% of MWCNT, depicting a thermal increment of 59.9% due to the well-established thread shaped MWCNT within the surface of SSD/SPDD for heat transfer. With further increase of MWCNT at 0.7 wt% & 0.9 wt% the thermal conductivity values drops to 0.672 W/m·K and 0.583 W/m·K. Maximum thermal conductivity increment of SSD/SPDD with MWCNT at a weight percentage of 0.1 wt%, 0.3 wt%, 0.5 wt%, 0.7 wt% and 0.9 wt% corresponds to 3.66%, 23.21%, 59.91%, 44.82% and 25.64%, respectively. High concentration of MWCNT with EPCM resulted in reduced intermolecular free movement of particles. This phenomena cause uncertainty in distribution of MWCNT and causes agglomeration, leading to reduction of heat transfer propagation ability of the prepared nanocomposite EPCM samples[8].

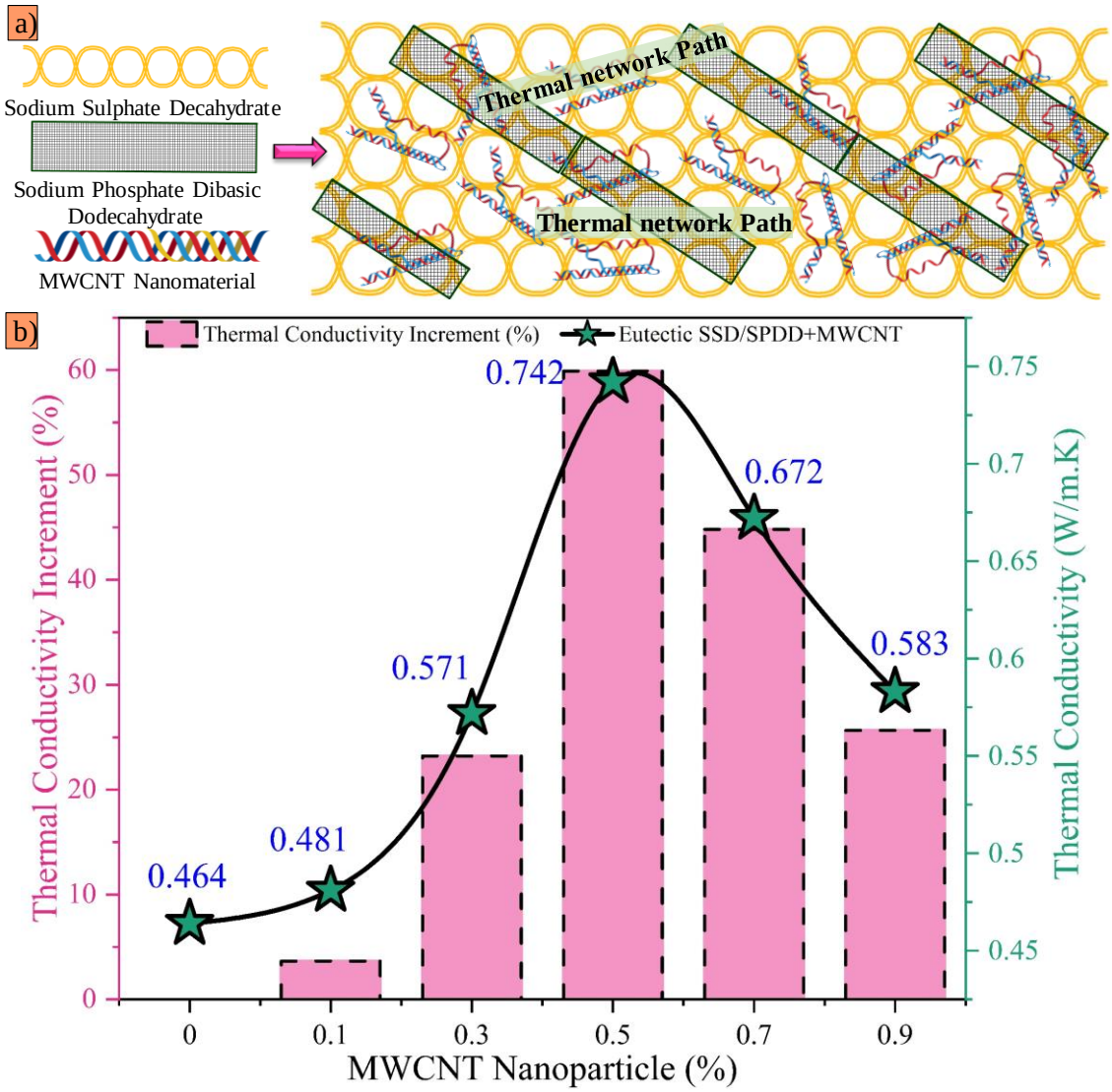

Figure 7: MWCNT penetrated SSD/SPDD a) Heat propagation mechanism; b) Thermal conductivity improvement value

3.6 Heat storage performance of MWCNT based EPCM

Thermal properties of the developed SSD/SPDD binary EPCM, and all nano composite with different weight percent of MWCNT samples were experimentally characterized using DSC instrument. Properties like phase transition temperatures, melting & freezing enthalpy and degree of supercooling of the nanocomposite PCM were examined through DSC analysis. Subsequently, using the melting and freezing enthalpy of the developed nanocomposite sample energy storage efficiency is calculated. Equation (4) provides the numerical relation for energy storage efficiency (γ)[31]

$$\gamma = \left(\frac{\Delta H_f}{\Delta H_m}\right) * 100\% \quad (4)$$

In equation (4), ΔH_m and ΔH_f denotes the melting and freezing enthalpy of nanocomposite PCM in J/g, during phase transition from solid to liquid and vice versa.

Figure 8 shows the heat flow curves (melting & freezing) of EPCM and its composite with various weight fraction of MWCNT nanoparticle. Additionally, Table 1 provides more information on melting point, freezing point, phase transition enthalpy and degree of supercooling for the developed base and nanocomposite PCM. In prior to the discussion on energy storage ability of MWCNT penetrated SSD/SPDD, it is important to analyse and compare the experimentally determined values of SSD/SPDD with the numerically designed value in *Section 3.1*. SSD/SPDD binary EPCM has been designed and developed based on Schrader's equation in this research work. As per design calculation, we obtain SSD/SPDD at a eutectic composition of 62/38 wt% with phase transition temperature of 27.8 °C and melting enthalpy of 215 J/g. Similarly, it is evident that the developed SSD/SPDD binary EPCM has an onset melting temperature of 28.7 °C (~ equal to the designed value) along with melting enthalpy of 217.1 J/g. The above values ensures the reliability of the design and the close resemblance of thermal properties of the developed binary EPCM. In addition a single endothermic peak (composition SSD and SPDD individual has different endothermic peaks) is noticed in melting curve, which further enhances the reliability of developed EPCM.

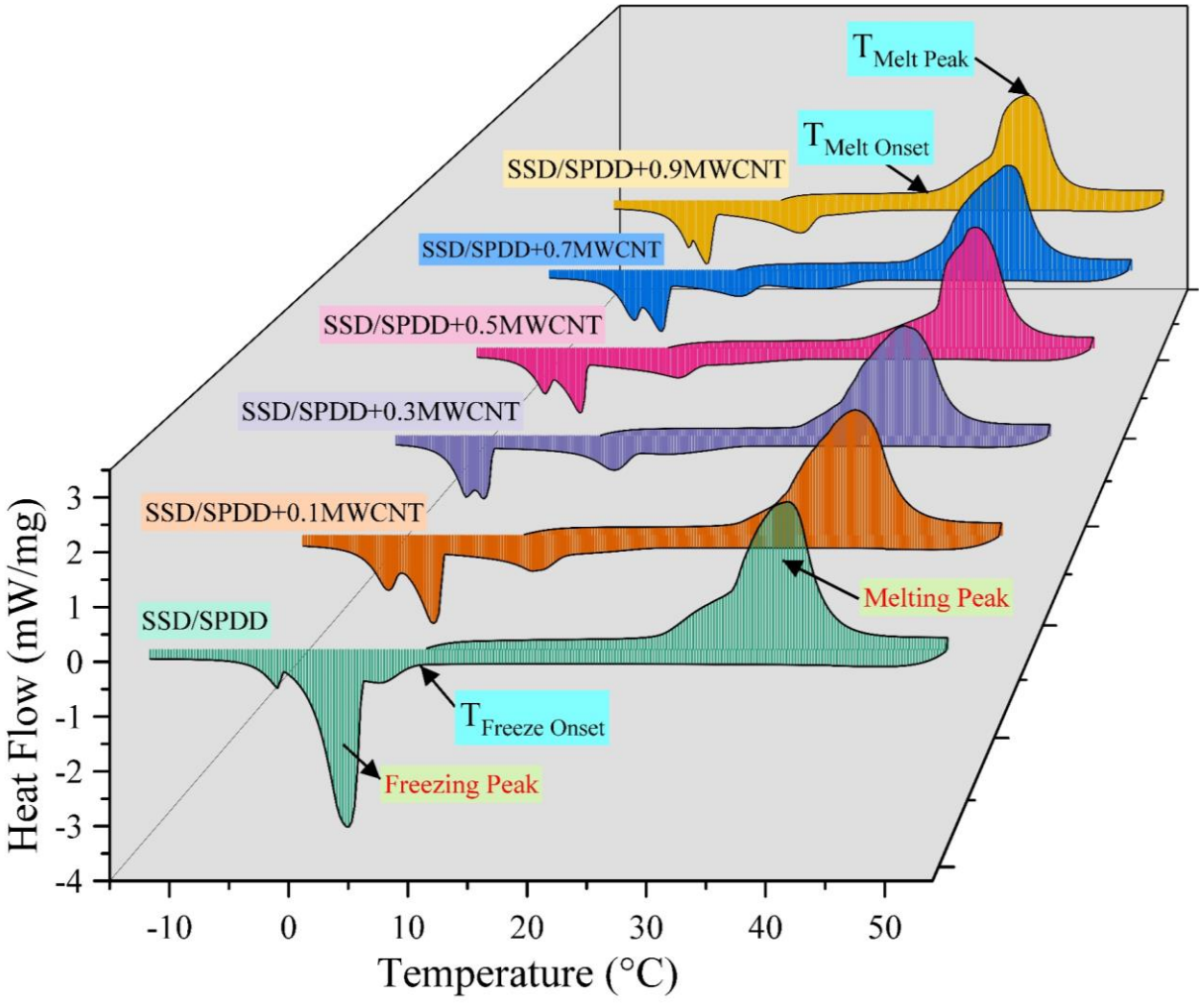

Figure 8: Thermophyscial properties of MWCNT penetrated SSD/SPDD melting and cooling enthalpy curves of SSD/SPDD+MWCNT

Table 1: Thermophysical parameters of MWCNT dispersed nanocomposite EPCM

Nano composite EPCM	*Heat Storage*			*Heat Release*			*Degree of Supercooling* ΔT_s *(°C)*
	$T_m\ (°C)\ (Onset)$	$T_m\ (°C)\ (Peak)$	$\Delta H_m\ (J/g)$	$T_f\ (°C)\ (Onset)$	$T_f\ (°C)\ (Peak)$	$\Delta H_f\ (J/g)$	
SSD/SPDD	*28.7*	*41.2*	*217.1*	*12.2*	*4.7*	*-148.2*	*16.5*
SSD/SPDD+0.1MWCNT	*27.4*	*41.6*	*225.2*	*23.2*	*3.1*	*-140.5*	*4.2*
SSD/SPDD+0.3MWCNT	*27.9*	*41.9*	*219.3*	*24.3*	*2.1*	*-132.1*	*3.6*
SSD/SPDD+0.5MWCNT	*27.3*	*42.1*	*218.6*	*24.2*	*3.2*	*-133.2*	*3.1*
SSD/SPDD+0.7MWCNT	*27.6*	*41.7*	*215.8*	*25.4*	*3.4*	*-140.3*	*2.2*
SSD/SPDD+0.9MWCNT	*27.1*	*38.6*	*212.1*	*22.7*	*2.2*	*-129.8*	*4.4*

To further enhance the thermal performance of the developed EPCM, MWCNT nanomaterial is dispersed at different weight fraction. Four important thermal properties to discuss in the DSC heat flow curves are a) Melting point, b) Melting enthalpy, c) Freezing enthalpy and d) Degree of supercooling. Onset melting temperature denotes the initialization of melting process with heat energy supply, and it can be inferred from the numerical values in Table 1, that for all nanocomposites the onset melting temperature are on close resemblance to that of the base EPCM. A single melting peak and three cooling peaks in the heat flow curves is observed, as the solid-liquid transition temperature is very nearer to the melting point of liquid phase a single peak is noticed; on the contrary during solidification, the liquid-solid transition depicts undercooling resulting in multiple peaks[43]. As well, the peak temperature are also similar to the base SSD/SPDD eutectic composite confirming no significant role of MWCNT in varying the phase transition temperature of the nanocomposite as their weight fraction is very minimal. The small variation observed in the onset peak and melting peak of MWCNT dispersed SSD/SPDD may be ascribed due to the interaction between MWCNT and SSD/SPDD as well owing to the isotropic structure of MWCNT nanoparticles[8]. Next, the melting enthalpy of MWCNT penetrated SSD/SPDD is explored, with inclusion of MWCNT a growing drift on the latent heat of the developed nanocomposite with 0.1 wt% MWCNT (225.2 J/g) is noticed. Likewise, increase in weight percent of MWCNT with SSD/SPDD the enthalpy decreases up to 212.1 J/g for 0.9 wt% MWCNT. In the above case, two phenomenon is expected to occur a) with MWCNT penetrated within the surface of SSD/SPDD, their intermolecular force of attraction surges as the nano sized thread shaped MWCNT are specialized in framing thermal networks and close bonds[44] b) mass of thermal energy storing PCM is replaced by fraction of MWCNT nanoparticle. At low weight fraction of MWCNT, the former phenomenon is significant and the melting enthalpy increases. Whereas on further

inclusion of MWCNT above 1.0 wt% the later phenomena is significant and slowly causes decrease of melting enthalpy. Subsequently, the exothermic peaks from Figure 8 shows multiple peaks, and lower enthalpy values, which is concern worth discussing. For every PCM acting as thermal batteries for energy storage, it is very important to supply the storage energy without losses. Nonetheless, the heat storage efficiency of the developed composite are 68.2% for SSD/SPDD, 62.3% for SSD/SPDD+0.1MWCNT, 60.2% for SSD/SPDD+0.3MWCNT, 60.9% for SSD/SPDD+0.5MWCNT, 65% for SSD/SPDD+0.7MWCNT and 61.1% for SSD/SPDD+0.9MWCNT. As per the second law of thermodynamics, there is always some loss expected to occur in a thermal system, and here the loss in energy is due to the loss in water molecules during the heating of samples under DSC until 55 °C. Whereas in the real time application of building heating and cooling the operating temperature is below 45 °C. Finally, the effect of MWCNT in reducing the degree of supercooling is analysed. All PCMs are anticipated to freeze back at their onset melting temperature for effective extraction of the stored heat energy, which is a significant problem in salt hydrate based PCM as they do not freeze at the onset melt temperature. Difference between onset melt temperature and onset freeze temperature is termed as degree of supercooling ΔT_s (°C). In general nucleating agents are included to suppress the degree of supercooling with salt hydrate PCM, although in the current investigation, to understand the effect of MWCNT with SSD/SPSS EPCM no nucleating agent is added. Clearly the numerical values in Table 1 indicates the reduction in degree of supercooling of SSD/SPDD from 16.5 °C to 2.2 °C. This phenomena is due to the uniform dispersion of MWCNT within the SSD/SPDD PCM in liquid state. MWCNT provides an initial provision for crystallization to develop and promote heterogeneous nucleation and causes the nanocomposite to freeze back at their designated temperature. Though the ΔT_s is not completely supressed, the reduction in ΔT_s obtained for the developed MWCNT penetrated SSD/SPDD is significant.

From the above discussion it can be inferred that SSD/SPDD+0.5MWCNT, contributes to 59.9% increment in thermal conductivity, non-comprising latent heat value (218.6 J/g) with 3.1 °C ΔT_s and 60.9% of heat storage efficiency can be actively preferred for real time TES applications.

3.7 Cycle stability analysis of MWCNT dispersed SSD/SPDD

PCMs are actively used for TES via waste heat recovery. During the process, the developed composite PCMs are subjected to repeated heating and cooling during which energy transfers occurs. Hence it is worth investigating the performance of the developed SSD/SPDD

binary EPCM, and MWCNT penetrated SSD/SPDD composite PCM at optimum concentration. Based on the thermal properties results, it can be inferred that SSD/SPDD+0.5MWCNT offers better thermal conductivity increment without compensation in latent heat potential. In this section, the chemical, optical and thermal property of SSD/SPDD+0.5MWCNT after 200 number of thermal cycles is evaluated. Thermal cycling is conducted manually for the nanocomposite PCM between temperature ranges of 10 °C to 60 °C ensuring complete phase transition. Figure 9 shows the characterization results of SSD/SPDD+0.5MWCNT after 200 thermal cycles evaluated using FTIR spectroscopy, UV-Vis spectroscopy and DSC.

For any pure and nanocomposite PCM, thermal properties like heat storage enthalpy and phase transition temperature decreases over repeated thermal cycles for two specific reasons a) presence of impurity & b) degradation of certain composition in the nanocomposite[45]. FTIR spectral curve analysis from Figure 9a shows similar peak between MWCNT dispersed composite PCM for 0 and 200 thermal cycles in a way that each peak fit onto another at the same frequency (sharp peaks at 487 cm^{-1}, 618 cm^{-1}, 987 cm^{-1} and 1078 cm^{-1}, weak peak at 1605-1714 cm^{-1} and an intense wide peak 2960-3580 cm^{-1}). Similar FTIR peaks ensures no composition of SSD/SPDD+0.5MWCNT to be degraded for the number of thermal cycles conducted. Added to the chemical stability is the optical absorbance and transmittance investigation. Figure 9b and 9c depicts the optical spectral curves of SSD/SPDD+0.5MWCNT after 200 thermal cycles, as it can be inferred that there is an increase in absorbance of the composite sample from 0.56 to 0.61 with repeated thermal cycling. The enhanced absorbance may be owing to better dispersion of MWCNT within the surface of SSD/SPDD composite PCM ensuring better response to absorb the incident photons. Likewise as transmissibility and absorbance of the composite samples are inversely proportional the transmissibility has been decrease from 27.55% to 24.00%. In order to evaluate the thermal characteristic of the developed nanocomposite, DSC analysis of the sample after 200 cycles is conducted and heat flow curves are plotted in Figure 9d. On further calculation the melting and cooling enthalpy of SSD/SPDD+0.5MWCNT after 200 cycle is 216.5 J/g and 113.2 J/g, whereas for nanocomposite without thermal cycling the latent heat during melting and cooling process is 218.6 J/g and 119.2 J/g. With repeated number of thermal cycles, the enthalpy of the developed nanocomposite is almost the same, ensuring that energy storage reliability of the nanocomposite. Nevertheless, the loss in melting enthalpy of the developed nanocomposite with repeated thermal cycles is owing to the presence of impurity with time. Similarly, for SSD/SPDD+0.5MWCNT after 200 cycle the onset melting point and the peak melting point

are identical. The aforementioned results clearly specifies the reliability of the developed MWCNT penetrated SSD/SPDD binary eutectic composite in terms of chemical stability, optical stability and thermal stability. Henceforth, the developed PCM is more likely to be opted for thermal management of buildings.

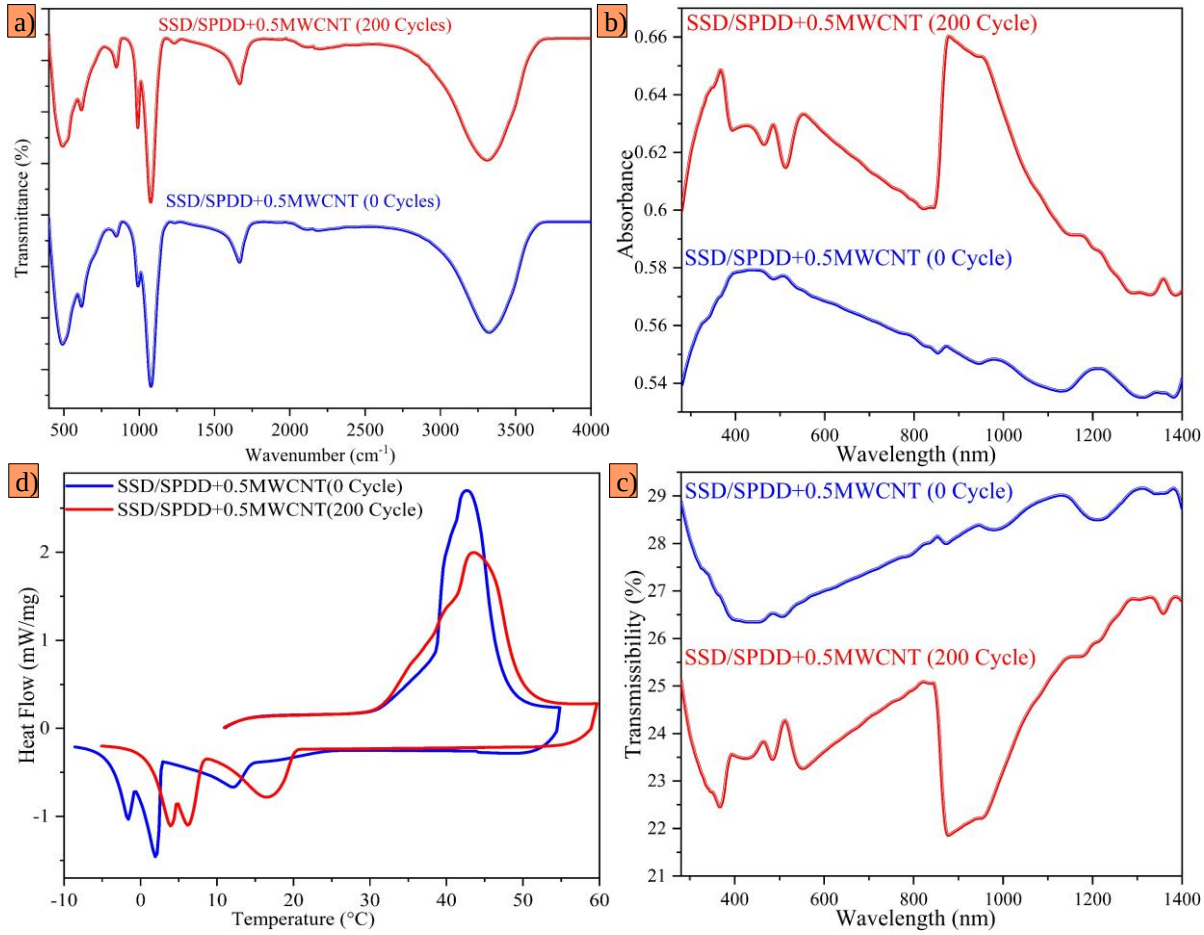

Figure 9: Cycle stability of MWCNT penetrated SSD/SPDD EPCM after 200 thermal cycles a) chemical stability spectral curve ; b) electromagnetic wave absorbance ; c) electromagnetic wave transmittance and d) Melting and cooling enthalpy

3.8 Numerical analysis of MWCNT dispersed binary EPCM

Using ANSYS workbench we numerically investigate the solidification/melting of eutectic salt hydrate PCM nanocomposite using two concentric tube as described in *Section 2.4*. As an outcome of the simulation, the temperature contour and mass fraction contour is evaluated. Figure 10a depicts the temperature contour of the concentric tube consisting of PCM and thermic fluid as a 3D representation, Figure 10b provides a zoom in visual of temperature plot and Figure 10c presents the mass fraction contour. Input parameters and the thermal property of base eutectic PCM SSD/SPDD and nanocomposite eutectic PCM SSD/SPDD+0.5 MWCNT used in the simulation of provided in (Supplementary Table T1-T2; Appendix III). All the results are depicted after applying the transient boundary condition for a duration of

500 second. As the developed PCM composite is intended for low temperature application, the heat input supplied is also less and an infinitesimal change in the temperature contour is observed in comparison between base EPCM, and PCM with MWCNT. For further understanding Figure 11 represents the variation in temperature of concentric tube in radial direction after a time period of 500 seconds. Figure 11a presents the temperature vs distance plot for SSD/SPDD as PCM, likewise Figure 11b presents the temperature vs distance plot for SSD/SPDD with MWCNT.

Initially, owing to the constant heat source at the outer surface of PCM tube, the PCM is melted and is at liquid state with charged thermal energy. As thermic fluid flows within the inner tube, thermal energy stored in PCM is supplied (discharged) to thermic flow. Henceforth, primarily we examine the temperature contour plot, where we witness EPCM in contact with the inner thermic fluid tube to discharge the stored thermal energy and starts crystallizing (solidifying) with drop in temperature of the PCM as can be inferred from the temperature contour colour change. Likewise, increase in temperature of the thermic fluid flowing is observed at region in close contact with the inner surface of the inner tube, as can be inferred from Figure 10b. To understand the influence of MWCNT in SSD/SPDD, a comparison on the temperature variation in the radial direction of concentric tube with base SSD/SPDD and with SSD/SPDD nanoparticle composite is provided in Figure 11. For better interpretation of the temperature variation, the changes in corresponding radial position are marked and discussed. As far as position A is concern, the base PCM discharge the stored heat quicker as their latent heat value is less compared to the MWCNT based PCM, and in the beginning of solidification process, nanoparticle tends to discharge all thermal energy. In regard to position B, MWCNT based PCM becomes predominant, as the channelized thermal networks of MWCNT owing to the enhanced thermal conductivity dissipate heat quicker than the based PCM.

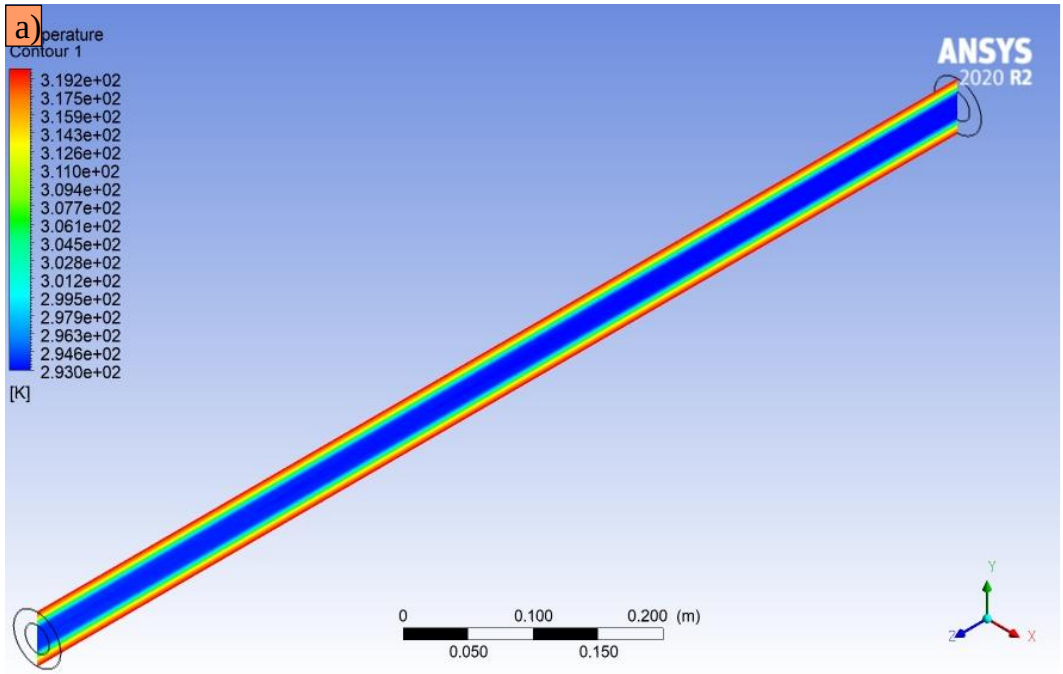
a)
perature
Contour 1
3.192e+02
3.175e+02
3.159e+02
3.143e+02
3.126e+02
3.110e+02
3.094e+02
3.077e+02
3.061e+02
3.045e+02
3.028e+02
3.012e+02
2.995e+02
2.979e+02
2.963e+02
2.946e+02
2.930e+02
[K]
ANSYS
2020 R2
0
0.100
0.200 (m)
0.050
0.150
Y
Z
X

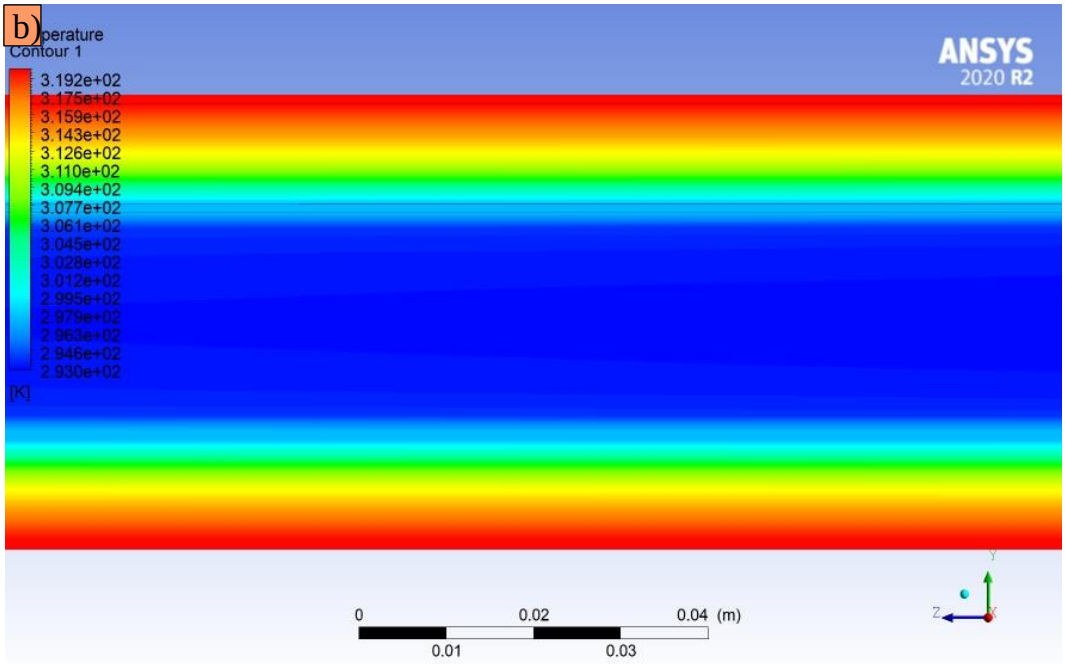
b)
perature
Contour 1
3.192e+02
3.175e+02
3.159e+02
3.143e+02
3.126e+02
3.110e+02
3.094e+02
3.077e+02
3.061e+02
3.045e+02
3.028e+02
3.012e+02
2.995e+02
2.979e+02
2.963e+02
2.946e+02
2.930e+02
[K]
ANSYS
2020 R2
0
0.02
0.04 (m)
0.01
0.03
Y
Z
X

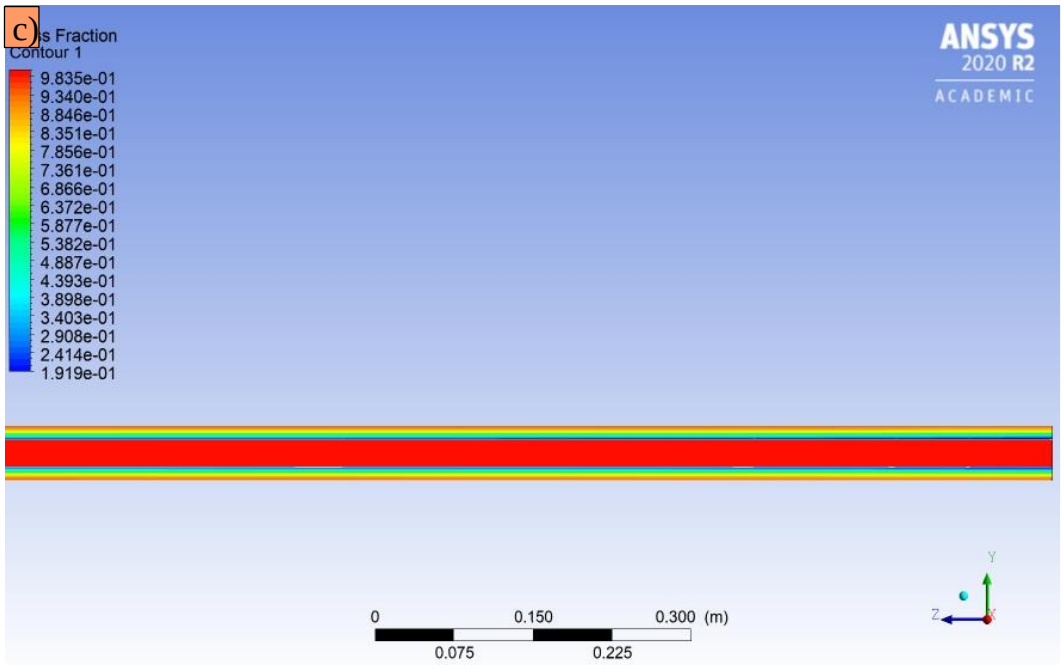
c)
s Fraction
Contour 1
9.835e-01
9.340e-01
8.846e-01
8.351e-01
7.856e-01
7.361e-01
6.866e-01
6.372e-01
5.877e-01
5.382e-01
4.887e-01
4.393e-01
3.898e-01
3.403e-01
2.908e-01
2.414e-01
1.919e-01
ANSYS
2020 R2
ACADEMIC
0
0.150
0.300 (m)
0.075
0.225
Y
Z
X

626

Figure 10: Numerical simulation results a) temperature contour plot of the system in 3 dimensional view; b) Zoom in temperature contour plot and c) Mass Fraction contour plot to understand the solidification/melting of PCM

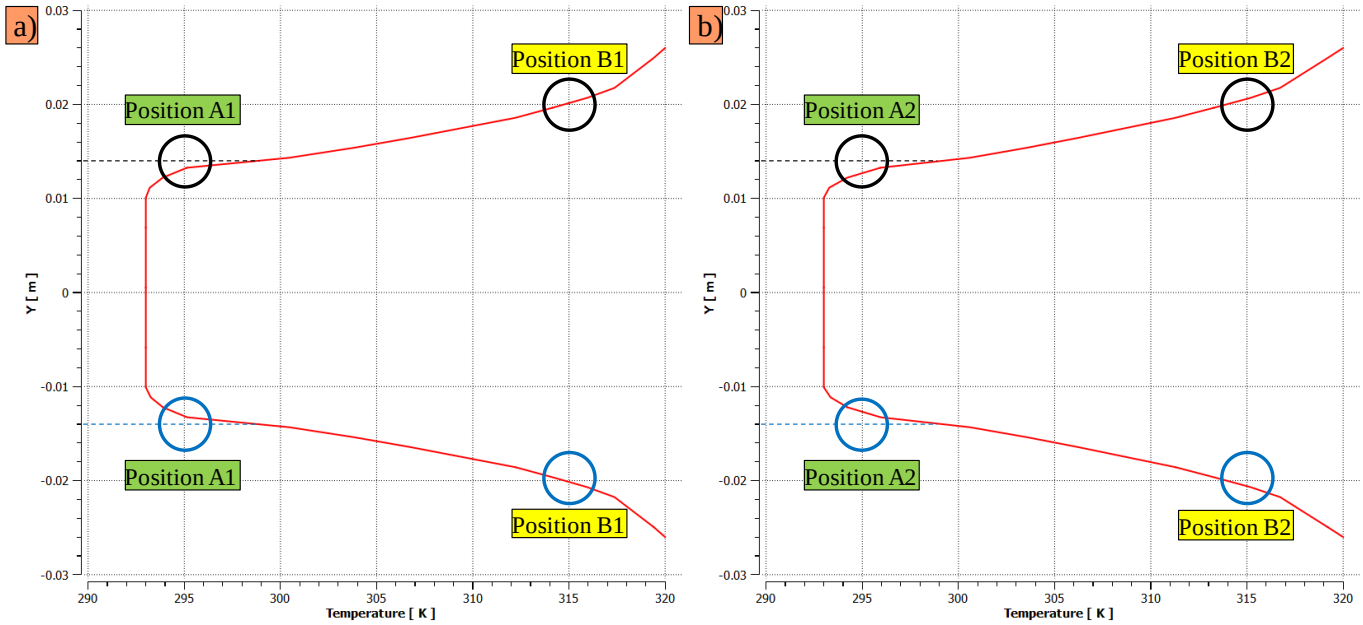

Figure 11: Variation in temperature in radial direction of concentric tube a) when filled with SSD/SPDD as PCM material; b) when filled with SSD/SPDD+0.5MWCNT nanocomposite as PCM.

Next significant result obtained is the mass fraction, as can be inferred from Figure 10c for MWCNT based PCM. Here we infer the percentage of PCM that has been solidified with discharging thermal energy to the thermic fluid after a flow period of 500 s. On keen analysis we see, PCM closer to the surface of outer tube exist in liquid state, which is owing to the constant heat input. Likewise, the thermic fluid remains in liquid state, as the primary focus of the application is only to warm the thermic fluid and not to heat it for phase transition from liquid to vapour. Based on further analysis we obtain the liquid fraction of base PCM to be 78.56% and MWCNT based PCM to be 71.42%. Due to the improved thermal conductivity of MWCNT based PCM, most the nanoparticle dispersed PCM liberated heat at a faster rate and undergoes phase transition, however the mass fraction of base PCM solidified is considerable lower, which can also be ascribed owing to the higher degree of supercooling. The numerical simulation conducted is envisioned to depict better understanding on the performance of PCM on integrating to a commercial system, as well results in (Supplementary S02-S13; Appendix III) provides more results on simulation of base eutectic PCM SSD/SPDD and nanocomposite eutectic PCM SSD/SPDD.

4.0 Corrosion Analysis

The main issue with salt hydrates is their propensity to corrode metals that come in reach with it. The corroded metal then diffuses into the salt hydrates' storage media, disrupting their thermal properties and weakening the final product. Protection against corrosion enhances the practicality and financial advantages of metals as well as the applicability of salt hydrate based PCM for energy storage. Since aluminium is one of the most used macro packing materials, a corrosion investigation was done using aluminium metal samples to determine its compatibility. Herewith, a circular aluminium plate of 20 mm diameter and 1 mm thickness is used as aluminium samples for testing, to analyse the corrosion effect of SSD/SPDD nanocomposite. Corrosion rate in Al metallic plate is analysed under a) ambient condition (kept in open atmosphere); b) SSD/SPDD eutectic salt hydrate PCM and c) SSD/SPDD+MWCNT nanocomposite eutectic salt hydrate PCM. Al metallic plate is engrossed within eutectic salt hydrate SSD/SPDD and SSD/SPDD+MWCNT in a glass beaker for the aforementioned cases. Corrosion analysis is conducted by placing the samples under salt hydrate exposure for a period of 3 months. The corrosion rate is analysed using the formula as in equation (5)[46] after 10 days, 30 days and 90 days to ensure whether the occurrence of corrosion is under permissible limit as per the ASTM standard or is very critical.

$$Corrosion\ rate = \frac{534*W}{A*T*D} \quad (5)$$

Where corrosion rate is determined in mpy (mills per year), W is the mass loss of metal in mg, A represents the surface area of metal in cm^2 (6.28 cm^2 for the Al sample), T indicates the exposure time in hours & D is the density of metal in g/cm^3 (2.7 for Al). Corrosion rate for each samples and their permissible limit is discussed in Table 2 with focus on weight loss of the sample at different environmental conditions. Figure 12 displays the SEM image of Al sample used for the corrosion analysis testing before exposed to the SSD/SPDD eutectic PCM.

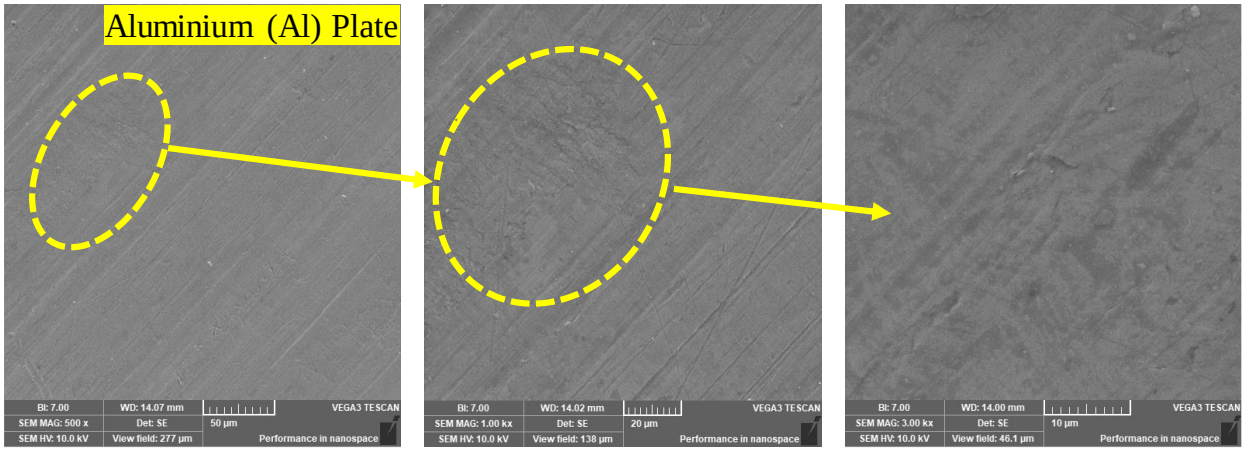

Figure 12: SEM visuals of aluminium plate before exposed to eutectic salt hydrate

Table 2: Corrosion rate analysis of aluminium sample under different environmental condition

Nature of environment	*Time duration* ***(hours)***	*Initial Mass* ***(mg)***	*Final Mass* ***(mg)***	*Mass loss* ***(mg)***	*Corrosion rate* ***(mpy)***	*Level of Corrosion**
Exposed to Ambient Condition	*240*	*810.8*	*810.8*	*0*	*0*	*Nil*
	720	*810.8*	*810.8*	*0*	*0*	*Nil*
	2160	*810.8*	*810.7*	*0.1*	*0.0015*	*Low*
Exposed to SSD/SPDD	*240*	*811.1*	*811.1*	*0*	*0*	*Nil*
	720	*811.1*	*810.8*	*0.3*	*0.0136*	*Low*
	2160	*811.1*	*809.9*	*1.2*	*0.0181*	*Low*
Exposed to SSD/SPDD + MWCNT	*240*	*812.2*	*812.2*	*0*	*0*	*Nil*
	720	*812.2*	*812.1*	*0.1*	*0.0045*	*Low*
	2160	*812.2*	*811.6*	*0.6*	*0.0091*	*Low*

** Severity of general corrosivity range (Low <2mpy); (Moderate 2-5mpy); (High 5-10mpy) and (Severe >10)*[47]

It is quite evident from Table 2, that on exposing the sample under different environmental condition the weight loss is very minimal and is within the permission limit. For Al sample endorsed under SSD/SPDD eutectic PCM the corrosion rate is 0.018 mpy after 90 days and with SSD/SPDD+MWCNT the corrosion rate is 0.009 mpy after 90 days. With SSD/SPDD eutectic PCM a selective leaching corrosion over the surface of metal is observed, however with inclusion of MWCNT, the interaction between salt hydrate crystals and Al metal surface is reduced thereby reducing corrosion. For percipience, the samples exposed under each condition were analysed using SEM image after 10days, 30days and 90 days and are displayed as in Figure 13. For Al sample exposed under ambient atmospheric corrosion no indication of corrosion is seen on a microscopic level. Whereas, for Al sample under eutectic salt hydrate SSD/SPDD we observe deposition of salt hydrate over the surface which slowly develops strains resulting in surface leaching leading to corrosion, however the corrosion rate is under permissible limit. Subsequently for Al sample under nanocomposite eutectic PCM of SSD/SPDD+MWCNT we observe no indication of rust formation, as MWCNT suppress the interaction between salt hydrate and metal surface leading to corrosion. In addition to the above result to exhibit an enlightenment on the surface of Al sample digital images are provided as can be inferred in (Supplementary S14; Appendix IV).

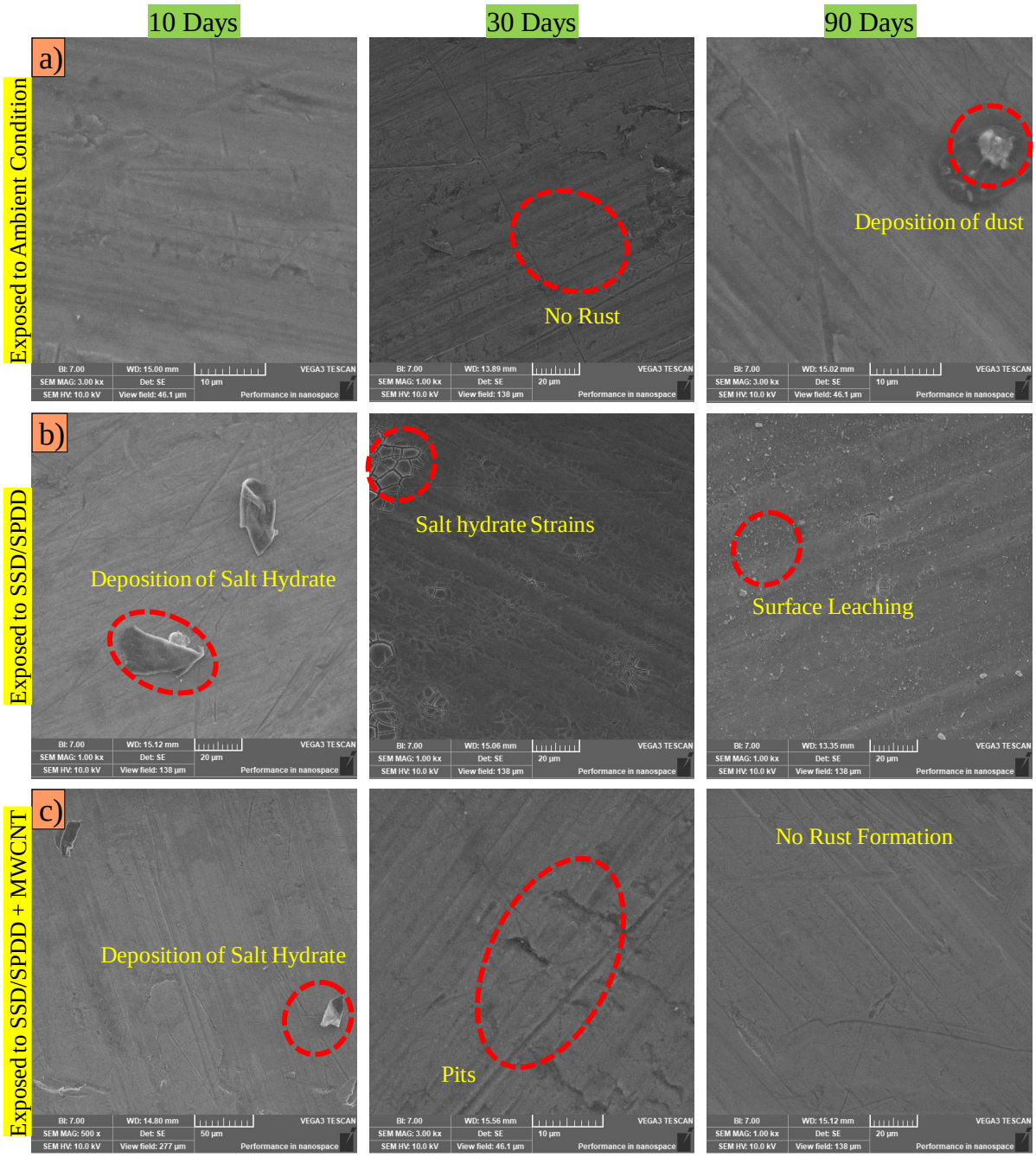

Figure 13: SEM visuals of aluminium plate on exposed to a) ambient atmospheric condition; b) SSD/SPDD; and c) SSD/SPDD+MWCNT nanocomposite eutectic PCM for 10days, 30 days and 90 days.

5.0 Conclusion

A novel low-temperature inorganic salt hydrate EPCM, specifically SSD/SPDD, was successfully developed using a straightforward process involving melting and sonication. To enhance its properties, multi-walled carbon nanotubes (MWCNT) were incorporated onto the surface of the developed SSD/SPDD EPCM, resulting in the SSD/SPDD+MWCNT nanocomposite. The microstructure, chemical composition, optical characteristics and thermal

properties were comprehensively analysed through SEM visual examination, FTIR spectral analysis, UV-Vis absorbance and transmittance measurements, temperature-dependent heat behaviour (THB) and heat flow analysis using DSC. The following conclusions were drawn from these analyses: The eutectic composition of SSD/SPDD comprises 62% of SSD and 38% of SPDD. This composition results in an equivalent eutectic melting of 27.8 °C and a corresponding melting enthalpy of 215 J/g. With the inclusion of MWCNT nanoparticles, the FTIR spectral reveals improved chemical stability, as evidenced by the absence of new peaks or chemical reactions. Simultaneously, the UV-Vis spectral analysis demonstrates a significant increase in absorbance from 0.17 to 0.78, representing a 500% enhancement, along with a decrease in transmissibility from 74.2% to 16.4%. Furthermore, the incorporation of 0.5 wt% MWCNT with SSD/SPDD results in a remarkable 59.9% increase in the thermal conductivity of the developed nanocomposite. This enhancement can be attributed to the MWCNT's ability to penetrate SSD/SPDD surface and establish well-connected thermal network, a phenomenon supported by the visual observations of the material's morphology. The DSC heat flow curves confirmed the stability of the phase transition temperature and energy storage ability, with no discernible compensation effects due to the intermolecular force of attraction between MWCNT and SSD/SPDD. Furthermore, the presence of MWCNT facilitated the liquid-phase EPCM to crystallize and starts freezing at their melting temperature, resulting in a reduced degree of supercooling.

After subjecting the material to 200 heating and cooling cycles, the energy storage capacity and optical absorbance showed minimal variations, staying within a 10% range. Additionally, FTIR spectral analysis showed intense peaks attributed to the evaporation of hydrate molecules, which occurred as the thermal cycling was conducted in an open atmosphere. The ANSYS simulation results, including mass fraction and temperature contour plots under transient boundary conditions, provide valuable insights into the heat transfer rate and effectiveness of the developed MWCNT@SSD/SPDD nanocomposite for energy storage applications. Similarly, the corrosion analysis conducted on the developed nanocomposite binary eutectic sample SSD/SPDD+MWCNT, during a 90-day contact period with aluminium metal, reveals a low corrosion rate of 0.009 mpy. This low rate is attributed to MWCNT's ability to reduce the interaction between SSD/SPDD and the aluminium metal surface, thereby expanding the real-time applications of eutectic salt hydrate PCM.

Acknowledgement

Authors acknowledges the financial assistance of Sunway University through Sunway University's International Research Network Grant Scheme 2.0 (IRNGS 2.0) 2022 (STR-IRNGS-SET-RCNMET-01-2021) for carrying out this research.

References

1. Zalba, B.; Marın, J. M.; Cabeza, L. F.; Mehling, H., Review on thermal energy storage with phase change: materials, heat transfer analysis and applications. *Applied thermal engineering* **2003,** *23* (3), 251-283.
2. Kaygusuz, K., The viability of thermal energy storage. *Energy Sources* **1999,** *21* (8), 745-755.
3. Tyagi, V.; Chopra, K.; Kalidasan, B.; Chauhan, A.; Stritih, U.; Anand, S.; Pandey, A.; Sarı, A.; Kothari, R., Phase change material based advance solar thermal energy storage systems for building heating and cooling applications: A prospective research approach. *Sustainable Energy Technologies and Assessments* **2021,** *47*, 101318.
4. Kalidasan, B.; Pandey, A.; Shahabuddin, S.; Samykano, M.; Thirugnanasambandam, M.; Saidur, R., Phase change materials integrated solar thermal energy systems: global trends and current practices in experimental approaches. *Journal of Energy Storage* **2020,** *27*, 101118.
5. Pandey, A.; Hossain, M.; Tyagi, V.; Abd Rahim, N.; Jeyraj, A.; Selvaraj, L.; Sari, A., Novel approaches and recent developments on potential applications of phase change materials in solar energy. *Renewable and Sustainable Energy Reviews* **2018,** *82*, 281-323.
6. Amir, M.; Deshmukh, R. G.; Khalid, H. M.; Said, Z.; Raza, A.; Muyeen, S.; Nizami, A.-S.; Elavarasan, R. M.; Saidur, R.; Sopian, K., Energy storage technologies: An integrated survey of developments, global economical/environmental effects, optimal scheduling model, and sustainable adaption policies. *Journal of Energy Storage* **2023,** *72*, 108694.
7. Kalidasan, B.; Pandey, A.; Saidur, R.; Samykano, M.; Tyagi, V., Nano additive enhanced salt hydrate phase change materials for thermal energy storage. *International Materials Reviews* **2022**, 1-44.
8. Kumar, R.; Samykano, M.; Pandey, A.; Kadirgama, K.; Tyagi, V., A comparative study on thermophysical properties of functionalized and non-functionalized Multi-Walled Carbon Nano Tubes (MWCNTs) enhanced salt hydrate phase change material. *Solar Energy Materials and Solar Cells* **2022,** *240*, 111697.
9. Nazir, H.; Batool, M.; Ali, M.; Kannan, A. M., Fatty acids based eutectic phase change system for thermal energy storage applications. *Applied Thermal Engineering* **2018,** *142*, 466-475.
10. del Barrio, E. P.; Godin, A.; Duquesne, M.; Daranlot, J.; Jolly, J.; Alshaer, W.; Kouadio, T.; Sommier, A., Characterization of different sugar alcohols as phase change materials for thermal energy storage applications. *Solar Energy Materials and Solar Cells* **2017,** *159*, 560-569.
11. Li, G.; Zhang, B.; Li, X.; Zhou, Y.; Sun, Q.; Yun, Q., The preparation, characterization and modification of a new phase change material: CaCl2· 6H2O–MgCl2· 6H2O eutectic hydrate salt. *Solar Energy Materials and Solar Cells* **2014,** *126*, 51-55.
12. Zhang, C.; Zhang, Z.; Ye, R.; Gao, X.; Ling, Z., Characterization of MgCl2· 6H2O-based eutectic/expanded perlite composite phase change material with low thermal conductivity. *Materials* **2018,** *11* (12), 2369.
13. Shahbaz, K.; AlNashef, I.; Lin, R.; Hashim, M.; Mjalli, F.; Farid, M., A novel calcium chloride hexahydrate-based deep eutectic solvent as a phase change materials. *Solar Energy Materials and Solar Cells* **2016,** *155*, 147-154.
14. Liu, Y.; Yang, Y., Use of nano-α-Al2O3 to improve binary eutectic hydrated salt as phase change material. *Solar Energy Materials and Solar Cells* **2017,** *160*, 18-25.

15. Fang, Y.; Su, J.; Tang, Y.; Liang, X.; Wang, S.; Gao, X.; Zhang, Z., Form-stable Na2SO4· 10H2O-Na2HPO4· 12H2O eutectic/hydrophilic fumed silica composite phase change material with low supercooling and low thermal conductivity for indoor thermal comfort improvement. *International Journal of Energy Research* **2020,** *44* (4), 3171-3182.
16. Wu, Y.; Wang, T., The dependence of phase change enthalpy on the pore structure and interfacial groups in hydrated salts/silica composites via sol–gel. *Journal of colloid and interface science* **2015,** *448*, 100-105.
17. Liu, L.; Peng, B.; Yue, C.; Guo, M.; Zhang, M., Low-cost, shape-stabilized fly ash composite phase change material synthesized by using a facile process for building energy efficiency. *Materials Chemistry and Physics* **2019,** *222*, 87-95.
18. Xin, W.; Fang, J.; Jiang, W.; Ping, L.; Na, L.; Yanhan, F.; Wang, L., Preparation and modification of novel phase change material Na2SO4· 10H2O-Na2HPO4· 12H2O binary eutectic hydrate salt. *Energy Sources, Part A: Recovery, Utilization, and Environmental Effects* **2022,** *44* (1), 1842-1853.
19. Liu, Y.; Yang, Y., Preparation and thermal properties of Na2CO3· 10H2O-Na2HPO4· 12H2O eutectic hydrate salt as a novel phase change material for energy storage. *Applied Thermal Engineering* **2017,** *112*, 606-609.
20. Liu, Y.; Yang, Y., Form-stable phase change material based on Na2CO3· 10H2O-Na2HPO4· 12H2O eutectic hydrated salt/expanded graphite oxide composite: the influence of chemical structures of expanded graphite oxide. *Renewable energy* **2018,** *115*, 734-740.
21. Wu, Y.; Wang, T., Hydrated salts/expanded graphite composite with high thermal conductivity as a shape-stabilized phase change material for thermal energy storage. *Energy conversion and management* **2015,** *101*, 164-171.
22. Xie, N.; Niu, J.; Zhong, Y.; Gao, X.; Zhang, Z.; Fang, Y., Development of polyurethane acrylate coated salt hydrate/diatomite form-stable phase change material with enhanced thermal stability for building energy storage. *Construction and Building Materials* **2020,** *259*, 119714.
23. Zhang, Y.; Wang, J.; Yang, X.; Ali, H. M.; Said, Z.; Liu, C., Fabrication of shape-stabilized phase change materials based on waste plastics for energy storage. *Journal of Energy Storage* **2022,** *52*, 104973.
24. Ling, Z.; Liu, J.; Wang, Q.; Lin, W.; Fang, X.; Zhang, Z., MgCl2· 6H2O-Mg (NO3) 2· 6H2O eutectic/SiO2 composite phase change material with improved thermal reliability and enhanced thermal conductivity. *Solar Energy Materials and Solar Cells* **2017,** *172*, 195-201.
25. Xie, N.; Luo, J.; Li, Z.; Huang, Z.; Gao, X.; Fang, Y.; Zhang, Z., Salt hydrate/expanded vermiculite composite as a form-stable phase change material for building energy storage. *Solar Energy Materials and Solar Cells* **2019,** *189*, 33-42.
26. Zou, T.; Xu, T.; Cui, H.; Tao, H.; Xu, H.; Zhou, X.; Chen, Q.; Chen, J.; Huang, G.; Sun, Y., Super absorbent polymer as support for shape-stabilized composite phase change material containing Na2HPO4· 12H2O–K2HPO4· 3H2O eutectic hydrated salt. *Solar Energy Materials and Solar Cells* **2021,** *231*, 111334.
27. Yanping, Y.; Wenquan, T.; Xiaoling, C.; Li, B., Theoretic prediction of melting temperature and latent heat for a fatty acid eutectic mixture. *Journal of Chemical & Engineering Data* **2011,** *56* (6), 2889-2891.
28. Huang, X.; Alva, G.; Liu, L.; Fang, G., Preparation, characterization and thermal properties of fatty acid eutectics/bentonite/expanded graphite composites as novel form–stable thermal energy storage materials. *Solar Energy Materials and Solar Cells* **2017,** *166*, 157-166.
29. Ke, H., Phase diagrams, eutectic mass ratios and thermal energy storage properties of multiple fatty acid eutectics as novel solid-liquid phase change materials for storage and retrieval of thermal energy. *Applied Thermal Engineering* **2017,** *113*, 1319-1331.
30. Kalidasan, B.; Pandey, A.; Saidur, R.; Tyagi, S.; Mishra, Y. K., Experimental evaluation of binary and ternary eutectic phase change material for sustainable thermal energy storage. *Journal of Energy Storage* **2023,** *68*, 107707.

31. Kalidasan, B.; Pandey, A.; Saidur, R.; Kothari, R.; Sharma, K.; Tyagi, V., Eco-friendly coconut shell biochar based nano-inclusion for sustainable energy storage of binary eutectic salt hydrate phase change materials. *Solar Energy Materials and Solar Cells* **2023,** *262*, 112534.
32. Kalidasan, B.; Pandey, A.; Rahman, S.; Sharma, K.; Tyagi, V., Experimental Investigation of Graphene Nanoplatelets Enhanced Low Temperature Ternary Eutectic Salt Hydrate Phase Change Material. *Energies* **2023,** *16* (4), 1574.
33. Khan, M. A. S.; Ganguly, B., Can surface energy be a parameter to define morphological change of rock-salt crystals with additives? A first principles study. *CrystEngComm* **2013,** *15* (14), 2631-2639.
34. Zhang, Z.; Lian, Y.; Xu, X.; Xu, X.; Fang, G.; Gu, M., Synthesis and characterization of microencapsulated sodium sulfate decahydrate as phase change energy storage materials. *Applied Energy* **2019,** *255*, 113830.
35. Lin, N.; Li, C.; Zhang, D.; Li, Y.; Chen, J., Emerging phase change cold storage materials derived from sodium sulfate decahydrate. *Energy* **2022,** *245*, 123294.
36. Shen, Z.; Kwon, S.; Lee, H. L.; Toivakka, M.; Oh, K., Enhanced thermal energy storage performance of salt hydrate phase change material: effect of cellulose nanofibril and graphene nanoplatelet. *Solar Energy Materials and Solar Cells* **2021,** *225*, 111028.
37. Shen, Z.; Oh, K.; Kwon, S.; Toivakka, M.; Lee, H. L., Use of cellulose nanofibril (CNF)/silver nanoparticles (AgNPs) composite in salt hydrate phase change material for efficient thermal energy storage. *International Journal of Biological Macromolecules* **2021,** *174*, 402-412.
38. Esmaeilzadeh, Z.; Rezaei, B.; Mousavi Shoushtari, A.; Mojtahedi, M. R. M., Enhancing the Thermal Characteristics of Shape-Stabilized Phase Change Nanocomposite Nanofibers by Incorporation of Multiwalled Carbon Nanotubes within the Nanofibrous Structure. *Advances in Polymer Technology* **2018,** *37* (1), 185-193.
39. Yu, J.; Grossiord, N.; Koning, C. E.; Loos, J., Controlling the dispersion of multi-wall carbon nanotubes in aqueous surfactant solution. *Carbon* **2007,** *45* (3), 618-623.
40. Kumar, R.; Samykano, M.; Ngui, W.; Pandey, A.; Kalidasan, B.; Kadirgama, K.; Tyagi, V., Investigation of thermal performance and chemical stability of graphene enhanced phase change material for thermal energy storage. *Physics and Chemistry of the Earth, Parts A/B/C* **2022,** *128*, 103250.
41. Gueymard, C. A., The sun's total and spectral irradiance for solar energy applications and solar radiation models. *Solar energy* **2004,** *76* (4), 423-453.
42. Kibria, M.; Anisur, M.; Mahfuz, M.; Saidur, R.; Metselaar, I., A review on thermophysical properties of nanoparticle dispersed phase change materials. *Energy conversion and management* **2015,** *95*, 69-89.
43. Gong, S.; Cheng, X.; Li, Y.; Shi, D.; Wang, X.; Zhong, H., Enhancement of ceramic foam modified hierarchical Al2O3@ expanded graphite on thermal properties of 1-octadecanol phase change materials. *Journal of Energy Storage* **2019,** *26*, 101025.
44. Kalidasan, B.; Pandey, A.; Shahabuddin, S.; George, M.; Sharma, K.; Samykano, M.; Tyagi, V.; Saidur, R., Synthesis and characterization of conducting Polyaniline@ cobalt-Paraffin wax nanocomposite as nano-phase change material: Enhanced thermophysical properties. *Renewable Energy* **2021,** *173*, 1057-1069.
45. Yang, L.; Cao, X.; Zhang, N.; Xiang, B.; Zhang, Z.; Qian, B., Thermal reliability of typical fatty acids as phase change materials based on 10,000 accelerated thermal cycles. *Sustainable Cities and Society* **2019,** *46*, 101380.
46. Owate, I.; Ezi, C.; Avwiri, G., Impact of environmental conditions on sub-surface storage tanks (Part I). *Journal of Applied Sciences and Environmental Management* **2002,** *6* (2), 79-83.
47. Jaragh, A.; Al-Ahmad, A. W.; Prakash, S.; Al-Mutairi, A.; Mathew, A. In *Internal Corrosion Severity Ranking of Crude Oil Pipelines*, SPE Kuwait Oil and Gas Show and Conference, SPE: 2019; p D023S005R005.